

Research Articles: Systems/Circuits

Diversity of Ganglion Cell Responses to Saccade-like Image Shifts in the Primate Retina

<https://doi.org/10.1523/JNEUROSCI.1561-22.2023>

Cite as: J. Neurosci 2023; 10.1523/JNEUROSCI.1561-22.2023

Received: 16 August 2022

Revised: 12 April 2023

Accepted: 8 May 2023

This Early Release article has been peer-reviewed and accepted, but has not been through the composition and copyediting processes. The final version may differ slightly in style or formatting and will contain links to any extended data.

Alerts: Sign up at www.jneurosci.org/alerts to receive customized email alerts when the fully formatted version of this article is published.

1

2

3 **Diversity of Ganglion Cell Responses to Saccade-like** 4 **Image Shifts in the Primate Retina**

5

6 Steffen Krüppel^{1,2,3}, Mohammad H. Khani^{1,2,4}, Dimokratis Karamanlis^{1,2,4}, Yunus C. Erol^{1,2,4},
7 Sören J. Zapp^{1,2}, Matthias Mietsch^{5,6}, Dario A. Protti⁷, Fernando Rozenblit^{1,2}, Tim
8 Gollisch^{1,2,3,*}

9 ¹University Medical Center Göttingen, Department of Ophthalmology, Göttingen, Germany

10 ²Bernstein Center for Computational Neuroscience Göttingen, Göttingen, Germany

11 ³Cluster of Excellence “Multiscale Bioimaging: from Molecular Machines to Networks of
12 Excitable Cells” (MBExC), University of Göttingen, Göttingen, Germany

13 ⁴International Max Planck Research School for Neurosciences, Göttingen, Germany

14 ⁵German Primate Center, Laboratory Animal Science Unit, Göttingen, Germany

15 ⁶German Center for Cardiovascular Research, Partner Site Göttingen, Göttingen, Germany

16 ⁷The University of Sydney, School of Medical Sciences (Neuroscience), Sydney, NSW,
17 Australia

18 *Correspondence: tim.gollisch@med.uni-goettingen.de

19

20 **Abbreviated title:** Responses to image shifts in primate retina

21

22 **Acknowledgements**

23 This work was funded by the European Research Council (ERC) under the European Union’s
24 Horizon 2020 research and innovation programme (grant agreement number 724822), by
25 Boehringer Ingelheim Fonds, and by the Deutsche Forschungsgemeinschaft (DFG, German
26 Research Foundation) – project numbers 154113120 (SFB 889, project C01), 432680300
27 (SFB 1456, project B05), and 390729940 (Germany’s Excellence Strategy – EXC 2067/1).

28

29 **Abstract**

30 Saccades are a fundamental part of natural vision. They interrupt fixations of the visual gaze
31 and rapidly shift the image that falls onto the retina. These stimulus dynamics can cause
32 activation or suppression of different retinal ganglion cells, but how they affect the encoding
33 of visual information in different types of ganglion cells is largely unknown. Here, we
34 recorded spiking responses to saccade-like shifts of luminance gratings from ganglion cells in
35 isolated marmoset retinas and investigated how the activity depended on the combination of
36 pre- and post-saccadic images. All identified cell types, On and Off parasol and midget cells
37 as well as a type of Large Off cells, displayed distinct response patterns, including particular
38 sensitivity to either the pre- or the post-saccadic image or combinations thereof. In addition,
39 Off parasol and Large Off cells, but not On cells, showed pronounced sensitivity to whether
40 the image changed across the transition. Stimulus sensitivity of On cells could be explained
41 based on their responses to step changes in light intensity, whereas Off cells, in particular,
42 parasol and the Large Off cells, seem to be affected by additional interactions that are not
43 triggered during simple light-intensity flashes. Together, our data show that ganglion cells in
44 the primate retina are sensitive to different combinations of pre- and post-saccadic visual
45 stimuli. This contributes to the functional diversity of the retina's output signals and to
46 asymmetries between On and Off pathways and provides evidence of signal processing
47 beyond what is triggered by isolated steps in light intensity.

48 **Introduction**

49 Research in visual neuroscience is often motivated by features of natural stimuli, like contrast,
50 color, and dynamics of the visual environment. Fully natural stimuli, however, are so rich in
51 features that elicited neural responses can often be difficult to interpret. It has thus proven
52 useful to focus on a particular feature of natural stimuli and recreate it artificially in abstract
53 form (Karamanlis et al., 2022), like changes in brightness investigated with uniform grayscale
54 stimuli (Hartline, 1938), spatial structure at varying resolution with gratings (Enroth-Cugell
55 and Robson, 1966), or small objects of interest with moving spots of light (Lettvin et al.,
56 1959). A specific feature that dominates much of the dynamics of vision is given by
57 saccades—rapid eye or body movements that shift the point of fixation and occur multiple
58 times per second in humans (Yarbus, 1967). Saccades strongly structure the visual stimuli that

59 fall onto the retina and thereby shape the neural signals sent from the eye to the rest of the
60 brain.

61 Retinal ganglion cells can display diminished responsiveness during saccades or saccade-like
62 image shifts, which is thought to contribute to saccadic suppression—the phenomenon of
63 reduced visual perception around the time of saccades (Roska and Werblin, 2003; Wurtz,
64 2008; Idrees et al., 2020). However, psychophysical studies have found that saccade
65 kinematics can be re-adjusted during the saccade if the target is moved at saccade onset
66 (Gaveau et al., 2003), indicating that meaningful visual processing must occur during
67 saccades. Indeed, suppression does not affect all retinal ganglion cells. Instead cells can
68 exhibit various responses to and during saccades (Noda and Adey, 1974; Amthor et al., 2005;
69 Sivyer et al., 2019), and responses after saccade offset may furthermore be particularly
70 informative about the newly fixated image (Segev et al., 2007; Krishnamoorthy et al., 2017).
71 For macaque ganglion cells, a study found responses to natural scenes to be strongly shaped
72 by the eye-movement-like temporal structure of the stimulus (Schottdorf and Lee, 2021).

73 Little is known, however, about how the rapid succession of fixations and brief transitions
74 affect the encoding of visual information, in particular for the primate retina. One hypothesis
75 might be that a saccade acts like a reset, allowing a new, independent snapshot of the visual
76 world after saccade offset. Retinal ganglion cells would then respond to the newly fixated
77 image according to how strongly the encountered visual contrast activates their receptive
78 fields. Yet, the offset of the previously fixated image also presents a potent stimulus just a few
79 tens of milliseconds earlier. In principle, ganglion cell activity after a saccade may thus
80 depend in a complex fashion on the combination of pre- and post-saccadic stimulus patterns
81 and be additionally influenced by the image motion during the saccade.

82 Here, we investigate how primate retinal ganglion cell responses to saccade-like image shifts
83 are shaped by the combination of pre- and post-saccadic stimulation of the receptive field.
84 Based on multielectrode-array recordings of ganglion cells from the marmoset retina and
85 functional identification of the major ganglion cell types, we find cell-type-specific
86 differences in the sensitivity to saccadic stimulus features. A model with nonlinear spatial
87 stimulus integration and response properties derived from simple light-intensity flashes could
88 partially capture these response characteristics. We conclude that saccades trigger cell-type-
89 specific signal-processing mechanisms that contribute to functional asymmetries between On
90 and Off ganglion cells and broaden the scope of visual features encoded by the retina across
91 saccades.

92 **Materials and Methods**

93 **Experimental Design and Statistical Analysis**

94 We used retinas of four adult marmoset monkeys (*Callithrix jacchus*) of either sex (3 male, 1
95 female), aged 4, 7, 10, and 15 years. Retinal tissue was obtained immediately after euthanasia
96 from animals used by other researchers, in accordance with national and institutional
97 guidelines and as approved by the institutional animal care committee of the German Primate
98 Center and by the responsible regional government office (Niedersächsisches Landesamt für
99 Verbraucherschutz und Lebensmittelsicherheit, permit number 33.19-42502-04-17/2496). For
100 each of the four retinas, we obtained one multielectrode-array recording of spiking activity
101 from individual retinal ganglion cells, yielding 80 to 600 cells per recording. No statistical
102 method was used to predetermine sample size. To compare performance of the investigated
103 computational models across the population of recorded cells, p-values were calculated using
104 the two-sided Wilcoxon signed-rank test implemented in the Python package SciPy.

105 **Tissue Preparation and Electrophysiology**

106 After enucleation, the eyes were dissected, and the cornea, lens, and vitreous humor were
107 carefully removed to gain direct access to the retina. The tissue was then transferred into a
108 light-tight chamber containing oxygenated (95% O₂ and 5% CO₂) Ames' medium (Sigma-
109 Aldrich, Munich, Germany), supplemented with 6 mM D-glucose, and buffered with 22 mM
110 NaHCO₃ to maintain a pH of 7.4. After 1-2 hours of dark adaptation, the retina was dissected
111 into smaller pieces. For each recording, a piece of peripheral retina was isolated from the
112 pigment epithelium and transferred to a multielectrode array (MultiChannel Systems,
113 Reutlingen, Germany; either 60 or 252-electrode planar arrays, 10 μm or 30 μm electrode
114 diameter and 100 μm minimum electrode spacing). The preparation was performed under
115 infrared illumination with a stereomicroscope equipped with night-vision goggles. During the
116 recording, the retina was perfused with the oxygenated Ames' medium (4-5 ml/min), and the
117 temperature of the recording chamber was kept constant around 33°C using an inline heater
118 (PH01, MultiChannel Systems, Reutlingen, Germany) and a heating element below the array.
119 The remaining retina tissue continued to be stored in the light-tight chamber and constantly
120 perfused with oxygenated Ames' medium for later recordings.

121 The multielectrode array signals were amplified, band-pass filtered (300 Hz to 5 kHz), and
122 stored digitally at 25 kHz (60-electrode arrays) or 10 kHz (252-electrode arrays), using the
123 software MC-Rack 4.6.2 (MultiChannel Systems). Spike sorting was performed with a

124 modified version of the sorting software Kilosort (Pachitariu et al., 2016), available at
125 <https://github.com/MouseLand/Kilosort> (original) and
126 <https://github.com/dimokaramanlis/KiloSortMEA> (modified version). The output of Kilosort
127 was visually inspected and manually curated with the software Phy2
128 (<https://github.com/cortex-lab/phy>). Only units with a well-separated cluster of voltage traces
129 and a clear refractory period were included for further analyses.

130 **Visual Stimulation**

131 Visual stimuli were generated by custom-made software written in C++ and OpenGL and
132 displayed on a gamma-corrected monochromatic white OLED monitor (eMagin) with a
133 refresh rate of 60 Hz and 800×600 pixels. The stimuli were projected onto the retina using a
134 telecentric lens (Edmund Optics), resulting in a pixel size of $7.5 \mu\text{m} \times 7.5 \mu\text{m}$ on the retina.
135 All stimuli used in this study had a mean light level of around 0.4, 0.9, or 3.3 mW/m²,
136 depending on the experiment, in the mesopic to low photopic regime. We calculated the
137 isomerization rates of the photoreceptors according to the formula presented in Lamb (1995),
138 using peak sensitivities and collecting areas ($0.37 \mu\text{m}^2$ for cones and $1 \mu\text{m}^2$ for rods) available
139 for marmoset and macaque (Travis et al., 1988; Schnapf et al., 1990; Tovée et al., 1992;
140 Schneeweis and Schnapf, 1995). The obtained rates were, for rods, around 540, 1050, and
141 3670 isomerizations per photoreceptor per second, respectively, for S-cones 30, 50, and 190,
142 and for M-cones 250, 610, and 2110. The same light level was also used for homogeneous
143 illumination between stimuli. Before the start of an experiment, the projection of the stimulus
144 screen was focused on the photoreceptor layer by visual inspection via a microscope.

145 **Estimation of Receptive Fields, Nonlinearities, and Autocorrelations**

146 In order to characterize the receptive fields of recorded cells and their autocorrelation
147 functions, a spatiotemporal binary white-noise stimulus on a checkerboard layout was
148 presented. Stimulus pixels had a size of $60 \mu\text{m}$ by $60 \mu\text{m}$ or $37.5 \mu\text{m}$ by $37.5 \mu\text{m}$ on the
149 retina. Each pixel was updated independently and pseudo-randomly at the monitor refresh rate
150 of 60 Hz to display either black or white (100% Michelson contrast). The stimulus consisted
151 of an alternating sequence of 1500 frames (25 s) of independent, non-repeating white noise
152 and 300 frames (5 s) of a fixed, repeated white-noise sequence. For the present study, only the
153 independent white-noise segments were used. The stimulus was presented for 30-40 minutes
154 leading to about 100,000 frames of independent white noise.

155 Receptive fields were determined by first calculating the spatiotemporal spike-triggered
156 average (STA) of a cell's responses to the independent white noise (Chichilnisky, 2001). We
157 used a temporal window of 30 frames (0.5 s) for the STA. To separate the STA into a
158 temporal and a spatial filter, we selected the element (pixel and time point) with the maximum
159 absolute value in the STA after smoothing with a spatial Gaussian filter of 60 μm standard
160 deviation. The temporal filter was then defined as the time course of the selected pixel in the
161 unsmoothed STA (normalized to unit Euclidean norm). The corresponding unsmoothed frame
162 was used to obtain the spatial filter by fitting a two-dimensional Gaussian to it. The Gaussian
163 fit is a customary way to reduce noise in the pixel-wise representation of the STA, and most
164 ganglion-cell receptive fields are well-fitted by the elliptical Gaussian. The standard deviation
165 of the Gaussian was then reduced to 80% of the original to account for the observation that
166 white-noise stimuli activate the surround less strongly than flashed stimuli and therefore often
167 overestimate the receptive field size relative to more flash-like stimuli with larger spatial
168 structure (Wienbar and Schwartz, 2018). The reduced Gaussian function was normalized to a
169 volume of unity and taken as an estimate of the receptive field, and the effective receptive-
170 field diameter was defined as the diameter of a circle with the same area as the 1.5-sigma
171 ellipse of this Gaussian function. Receptive-field outlines were displayed as this 1.5-sigma
172 ellipse.

173 The layouts of receptive fields were also used to confirm the location of the recorded retina
174 pieces as coming from the peripheral retina. To do so, we estimated the cell density of On and
175 Off parasol cells (see below for cell-type classification) by computing all nearest-neighbor
176 distances of receptive-field midpoints, finding the mode, and calculating the corresponding
177 density of a hexagonal grid with that node distance. We found densities of 60 to 120 On
178 parasol cells per mm^2 and 80 to 160 Off parasol cells per mm^2 , respectively, consistent with
179 the peripheral retina according to literature values (Gomes et al., 2005).

180 To characterize a cell's contrast-response relationship, we computed the cell's nonlinearity as
181 part of the linear-nonlinear model (Chichilnisky, 2001). This was done by computing the dot
182 product of every frame in the white-noise stimulus with the cell's normalized spatial filter and
183 convolving the resulting sequence with its normalized temporal filter to obtain a generator
184 signal for each stimulus frame. To reduce noise, the length of the temporal filter was cut to
185 0.25 s, and only pixels within the smallest rectangular window still containing the 3.75-sigma
186 ellipse of the Gaussian were included in this computation. The generator signals were then

187 binned into ten bins with equal number of data points, and the average spike count and
188 generator signal were calculated for each bin.

189 Spike-train autocorrelation functions were computed over 50 ms at a resolution of 0.04 ms
190 (25 kHz recordings) or 0.1 ms (10 kHz recordings) from the responses to the white-noise
191 stimulus, smoothed with a Gaussian filter with standard deviation of ten data points, and
192 normalized to a sum of unity.

193 **Classification of Retinal Ganglion Cells**

194 To be able to investigate whether different cell types play distinct roles during saccades, we
195 first classified cells manually in a way similar to the procedure in Field et al. (2007). For each
196 recording, we computed the first two principal components of all temporal filters. We then
197 constructed scatter plots of the projections of the temporal filters onto the first principal
198 component against the projection onto the second principal component as well as against the
199 effective receptive-field diameter. The scatter plots yielded clustered groups of cells,
200 corresponding to On and Off midget and parasol cells, respectively, and a fifth cell type that
201 we here call Large Off cells. Many recorded cells could readily be assigned to one of the
202 clusters based on these scatter plots. For cells which lay at the borders of clusters, assignment
203 to a cluster was additionally based on examining the spike-train autocorrelation function, the
204 detailed shapes of the temporal filter and the nonlinearity, the pixel-wise display of the spatial
205 component of the spike-triggered average, and the positioning of the receptive field relative to
206 receptive fields of other cells in the nearby clusters. While the autocorrelation function and
207 the estimated nonlinearity could often vary significantly within a cell type, the temporal filter
208 and tiling of visual space by the receptive fields could be used more reliably to further
209 distinguish cell types. Cells that could not be clearly assigned to one of the analyzed types
210 were excluded from further analyses. In total, this led to 842 analyzed out of 1172 recorded
211 cells. The 330 excluded cells were, presumably, mostly cells of types other than the five
212 identified cell types or too noisy to be classified.

213 **Saccadic Stimulus**

214 To stimulate the retina with saccade-like image shifts, we used a stimulus based on rapid
215 movements of a spatial square-wave grating. The grating had a Michelson contrast of 60%
216 and a bar width of 90 μm on the retina. The stimulus mimicked an alternating sequence of
217 fixations lasting 533 ms each and saccade-like transitions of 67 ms. During each fixation, the
218 grating remained static at one of four equally spaced spatial phases, which are called Positions

219 1, 2, 3, and 4. The sequence of positions was chosen pseudo-randomly. Transitions moved the
220 grating from one position to the next by translating the grating by about two full grating
221 periods, as previously used in (Krishnamoorthy et al., 2017). Note, however, that in our
222 experiments, these motion transitions were depicted for only four monitor frames such that
223 due to aliasing the screen did not show a smooth movement of the grating but rather a quick
224 succession of various grating positions. For half of the transitions, chosen pseudo-randomly,
225 the transition was masked by a uniform gray screen at mean intensity of the grating. The
226 saccadic stimulus was presented for 12-20 minutes resulting in 1200-2000 transitions.

227 We analyzed the responses of each cell to the transitions according to the combination of
228 grating position before the saccade, termed starting position, and the grating position after the
229 saccade, termed target position. For each of the resulting 16 combinations of starting and
230 target position, we collected the cell's responses to calculate a 350-ms-long peri-stimulus time
231 histogram (PSTH) with a bin size of 10 ms. For quantitative analyses of response amplitudes
232 just after the onset of the transition and after the onset of the new fixation, we divided each
233 PSTH into a first response window, ranging from 30 ms after onset of the transition until 10,
234 20, or 30 ms (selected manually for each experiment, depending on the response latencies
235 observed in that experiment) after onset of the target position, and a second response window
236 ranging from those 10-30 ms to 200 ms after onset of the target position. Peak responses in
237 each window were then determined after separately smoothing each corresponding PSTH
238 segment with a Gaussian of 20 ms standard deviation, using zero-padding.

239 The position of the boundary between the two response windows (10, 20, or 30 ms) was
240 determined with the goal of separating the observed early and late response peaks for all cells
241 that displayed such peaks (typically On parasol and midget as well as Off parasol cells). We
242 verified that response peak times for these cell types lay well within the considered response
243 windows with sufficient distance from the selected boundaries. For each of these cell types
244 and each response window, we examined the distribution of the time between response peak
245 and selected boundary and found that the average was similar to or larger than two standard
246 deviations in each case. We also checked that for Off midget cells, which had more sustained
247 responses with no obvious double-peak pattern, any response component that appeared to
248 solely relate to the starting position was contained in the first response window. Such a
249 response component is most easily identified in the transition that yields the strongest fixation
250 offset and weakest fixation onset response, that is, the transition with equal starting and target

251 position, both the opposite of the preferred target position. Large Off cells generally only
252 showed a single response event, which occurred well inside the second response window.

253 We collected the detected peak firing rates in each of the two response windows in two 4×4
254 response matrices, one for each response window. These response matrices were then Fourier-
255 transformed (two-dimensional discrete Fourier transform), yielding two complex-valued
256 matrices whose entries quantify the amplitudes and phases of different basic patterns in the
257 response matrices. We took the absolute values of the matrix entries, thereby disregarding the
258 phase and only keeping the amplitude of the patterns. From each transformed matrix, we
259 extracted the three entries (0, 1), (1, 0), and (3, 1), which correspond to specific sensitivities
260 (to target position, to starting position, and to change across the transition) as described in the
261 main text. These three entries were combined in a three-dimensional vector, yielding two
262 vectors for each cell that needed to be normalized in order to make them comparable across
263 cells. This was done by comparing the Frobenius norms of the two Fourier-transformed
264 response matrices and dividing both vectors by the larger one. Intuitively, this relates each
265 specific response modulation pattern to the total response modulation in the response window
266 with the stronger modulations. After having observed that three out of the six entries of the
267 two vectors are almost always close to zero, the remaining three values were combined into a
268 final sensitivity vector: the (0, 1) component, i.e. start sensitivity, of the vector of the first
269 response window, and the (1, 0) and (3, 1) components, i.e. target and change sensitivity, of
270 the vector of the second response window.

271 **Flashed Gratings**

272 As a means to judge the responses of cells to individually flashed gratings, we used a stimulus
273 that was designed to test the cells' responses to reversing gratings. The grating stimulus
274 started with one second of full-field mean light intensity gray after which a square-wave
275 grating with 100% Michelson contrast was presented. Every 0.2 seconds, the grating's
276 polarity was reversed, with 24 reversals in total. After the 25th grating presentation, the
277 stimulus returned to gray for one second before the next reversing grating started. The grating
278 size cycled through a list of bar widths of 7.5 μm , 15 μm , 30 μm , 60 μm , 120 μm , 240 μm ,
279 480 μm , and 6000 μm (full-field) in this order, and for each of those bar widths a specified
280 number of different spatial phases was tested – 1, 1, 2, 2, 4, 4, 8, and 1, respectively. For
281 example, the 30 μm grating was presented first at a relative spatial phase shift of 0°, then at a
282 shift of 90°. The entire paradigm was shown twice, taking about 5 minutes in total.

283 PSTHs for the onset and offset of the grating were calculated with a bin size of 10 ms for each
284 grating size irrespective of spatial phase. To display individual response traces, we calculated
285 the PSTHs from 0.3 s before until 0.4 s after onset, and from 0.4 s before until 0.3 s after
286 offset, respectively. For population analyses, only the 0.2 s after onset/offset were considered.
287 In this time window, the average firing rate was computed as a measure of response strength
288 for the grating onset and offset (rather than using the peak firing rate, which is more strongly
289 affected by noise from the small number of trials). Furthermore, to compare with the relative
290 sensitivities during the saccade stimulus, since the 90 μm bar width of the saccade stimulus
291 was not available in the reversing-grating data, the strengths for 60 μm and 120 μm were
292 averaged for grating onset and offset, respectively. Finally, we computed the relative strengths
293 of onset versus offset response and the relative sensitivity to target versus starting position
294 according to $(a - b)/(a + b)$, where a and b are the two response strengths (onset and
295 offset) or sensitivities (target and start).

296 In order to estimate the response quality of the cells (see section Cell Selection), we also
297 calculated PSTHs for the reversing part of the stimulus. PSTHs were calculated for a duration
298 of one reversing cycle (0.4 s) with a bin size of 10 ms, separately for each grating size and
299 grating phase, disregarding the first half cycle of the grating to reduce onset effects.

300 **Responses to Brightness Steps**

301 We used the responses of ganglion cells to full-field steps in light intensity as a basis for
302 modeling their responses to the saccadic stimulus. The light intensity steps lasted 0.5 s, going
303 alternatingly to white (+100% Michelson contrast) and black (-100% Michelson contrast),
304 separated by 1.5 s of gray mean-intensity illumination. This stimulus was repeated for 30-90
305 cycles, taking a total of 2-6 minutes. PSTHs were computed with a bin size of 10 ms both for
306 the entire cycle duration for display in the figures, and for a time window of 400 ms following
307 each of the four changes in light intensity for the modeling of responses to the saccadic
308 stimulus (see below).

309 **Modeling**

310 We compared the ability of two computational models to predict ganglion cell responses to
311 the saccadic stimulus based on a cell's responses to the brightness steps. For these analyses,
312 the transition period was modeled as homogeneous gray illumination at mean light intensity,
313 based on the observation that measured responses did not differ much between such masked
314 transitions and transitions with shifting grating position.

315 Both models use a weighted summation of the firing-rate profiles measured under brightness
 316 steps. The two models only differed in whether contrast signals over the receptive field were
 317 integrated linearly or nonlinearly when computing the weights. For the linear model, we first
 318 computed the net change in visual contrast over the receptive field for each transition in the
 319 saccade stimulus and used this as a weight for the corresponding response trace as measured
 320 under the brightness steps to arrive at the model prediction. Conversely, for the nonlinear
 321 model, we calculated a firing-rate prediction for each pixel individually according to its own
 322 contrast change, and only afterwards averaged over the receptive field, thus preventing the
 323 direct cancelation of activity by simultaneous brightening and darkening in the different parts
 324 of the receptive field.

325 Concretely, the two model predictions $R_{\text{linear}}(t)$ and $R_{\text{nonlinear}}(t)$ of a cell were computed
 326 from the cell's responses $R_{x \rightarrow y}(t)$ under brightness steps, where $x \rightarrow y$ stands for the different
 327 transitions white \rightarrow gray ($w \rightarrow g$), black \rightarrow gray ($b \rightarrow g$), gray \rightarrow white ($g \rightarrow w$), and gray \rightarrow black
 328 ($g \rightarrow b$). For a given transition from the pre-saccadic stimulus \vec{S}_{pre} to the post-saccadic
 329 stimulus \vec{S}_{post} , we used:

$$330 \quad R_{\text{linear}}(t) = \sum_{\text{all } x \rightarrow y} N(\vec{W} \cdot \vec{S}_n \cdot \sigma_{x \rightarrow y}) \cdot R_{x \rightarrow y}(t - d_n)$$

331 and

$$332 \quad R_{\text{nonlinear}}(t) = \sum_{\text{all } x \rightarrow y} \vec{W} \cdot N(\vec{S}_n \cdot \sigma_{x \rightarrow y}) \cdot R_{x \rightarrow y}(t - d_n)$$

333 Here, $N(\cdot)$ is a thresholding function, setting negative inputs to zero, and \vec{W} is the (Gaussian)
 334 receptive field of the cell (positive also for Off cells), evaluated at the pixel centers and
 335 correspondingly denoted as a vector. \vec{S}_n stands for the appropriate pixel-wise stimulus, \vec{S}_{pre}
 336 for the pre-saccadic image, used for $w \rightarrow g$ and $b \rightarrow g$, and \vec{S}_{post} for the post-saccadic image
 337 used for $g \rightarrow w$ and $g \rightarrow b$. The elements of the \vec{S}_n are -0.6 and 0.6 for dark and bright pixels,
 338 respectively, denoting the contrast values that were used in the saccadic stimulus. The time
 339 delay d_n is used to shift the responses corresponding to the occurrence of \vec{S}_{post} by the
 340 transition duration, hence $d_{\text{post}} = 67$ ms and $d_{\text{pre}} = 0$. The scalar factor $\sigma_{x \rightarrow y}$ is used to
 341 switch the sign of the stimulus elements when the contribution of a step from or to black is
 342 considered; hence $\sigma_{x \rightarrow y} = -1$ for $b \rightarrow g$ and for $g \rightarrow b$ and 1 otherwise. For the $R_{x \rightarrow y}(t)$, we
 343 used the 400 ms long PSTHs of the cell after the full-field brightness step from x to y as

344 calculated in the section “Responses to Brightness Steps” and zero-padded them for time
345 points outside of the 400 ms window.

346 Finally, for comparison with measured responses to the saccade stimulus, we allowed for a
347 constant latency shift that is applied in the same way to the firing-rate predictions for all 16
348 transitions. This aims at accounting for the overall faster responses under brightness steps,
349 owing to the higher contrast of this stimulus as compared to the saccade stimulus. We fitted
350 the latency shift for each cell by selecting the shift in the range of 0 to 50 ms with the
351 maximal Pearson correlation between the data and the prediction. For most cells, the latency
352 shift was less than 30 ms. Predictions were calculated for a 350 ms window starting at the
353 onset of the transition, which is the same duration as the PSTHs calculated for the saccadic
354 stimulus. For figures showing predicted responses, we jointly scaled the predictions for the 16
355 transitions to the same peak value as in the corresponding data from that cell, again to account
356 for differences in applied overall contrast.

357 We used two measures to evaluate the model performance. Firstly, we compared the response
358 matrices calculated from the predicted responses with the cell’s experimental response
359 matrices using a modified coefficient of determination. The modeled response matrices were
360 scaled to the same mean as the experimental ones to accommodate for the different contrasts.
361 The modified coefficient of determination between one pair of experimental and modeled
362 response matrices was then calculated as

$$363 \quad R^2 = 1 - \frac{\sum_{i,j}(m_{i,j}^{data} - m_{i,j}^{model})^2}{\sum_{i,j}(m_{i,j}^{data})^2}$$

364 where $m_{i,j}$ are the entries of the response matrix of the experimental data or of the prediction,
365 respectively. This modified coefficient of determination corresponds to substituting the mean
366 of the data’s response matrix in the denominator of the regular coefficient of determination
367 with zero. This effectively uses the total response strength as a signal rather than the deviation
368 from the mean and avoids that the denominator goes to zero for cells that respond equally to
369 all transitions.

370 Furthermore, we used the Euclidean distance in the three-dimensional sensitivity vector space
371 as a measure for model performance. The distance was computed between the sensitivity
372 vector as calculated from the model predictions and the sensitivity vector of the experimental
373 data. A low distance indicates that the coding properties have been reproduced well by the
374 model.

375 **Cell Selection**

376 In addition to excluding cells that could not be matched to one of the five analyzed cell types
377 as noted above, we excluded cells from further analyses that responded unreliably during the
378 relevant stimuli. To measure a cell's reliability during the saccadic stimulus, we first split its
379 responses into odd and even trials and calculated PSTHs individually. We then linked the 16
380 PSTHs of different starting and target position combinations together to generate a single
381 PSTH for all odd trials and a single PSTH for all even trials. Next, we computed the
382 coefficient of determination R^2 between the odd PSTH as data and the even PSTH as
383 prediction, and vice versa, and averaged these two values (Karamanlis and Gollisch, 2021).
384 Any cell with an averaged R^2 below 0.2 for the saccadic stimulus was excluded from all
385 analyses using that stimulus. In total, we analyzed the saccade responses of 166 On parasol,
386 41 On midget, 182 Off parasol, 51 Off midget, and 13 Large Off cells from four experiments.

387 For the analyses of the flashed-grating responses, we calculated the reliability similarly by
388 computing PSTHs of the reversing part of the stimulus separately for the first and second
389 presentation of the stimulus, linking the PSTHs of the different grating sizes and phases
390 together, and computing the coefficient of determination R^2 between the two PSTHs as above.
391 For this part of the analysis, we considered all cells with an averaged R^2 above 0.2 for the
392 reversing-gratings stimulus. This led to 151 On parasol, 49 On midget, 154 Off parasol, 40
393 Off midget, and 6 Large Off cells for the flashed-grating analysis.

394 For modeling responses to the saccadic stimulus, cells had to be sufficiently reliable during
395 both the saccadic as well as the full-field-brightness-steps stimulus. For calculating the
396 reliability during the full-field brightness steps, we proceeded similarly as above, but only
397 considered the 400 ms after any brightness change in order to exclude long periods without
398 changes in the stimulus. Again, we determined all cells with an averaged R^2 above 0.2 to be
399 reliable enough, leading to 122 On parasol, 25 On midget, 144 Off parasol, 37 Off midget,
400 and 11 Large Off cells for the modeling part of our analysis.

401 **Data Availability**

402 The spike-train data recorded for this work have been made publicly available at [https://gin.g-](https://gin.g-node.org/gollischlab/Krueppel_etal_2023_Marmoset_RGC_spiketrains_to_saccadic_shifts)
403 [node.org/gollischlab/Krueppel_etal_2023_Marmoset_RGC_spiketrains_to_saccadic_shifts](https://gin.g-node.org/gollischlab/Krueppel_etal_2023_Marmoset_RGC_spiketrains_to_saccadic_shifts)
404 (doi: 10.12751/g-node.thlt1j).

405 **Results**

406 **Stimulus and Analysis**

407 Saccades form rapid transitions between fixated images, and elicited responses in neurons of
408 the visual system may be influenced by the pre-saccadic image, the post-saccadic image, and
409 the transition in between. In order to investigate the coding properties of ganglion cells in the
410 primate retina under saccade-like image transitions, we recorded ganglion cell spiking activity
411 in isolated marmoset retinas with multielectrode arrays while projecting a saccade-like
412 stimulus onto the photoreceptors. To systematically probe transitions between different
413 illumination patterns inside the receptive fields of different ganglion cells, we chose a square-
414 wave luminance grating with a bar width of 90 μm as the spatial layout of the stimulus.
415 Taking into account the size of the marmoset eye (Troilo et al., 1993), this corresponds to
416 approximately 0.9° visual angle or, for example, a 10 cm thick tree branch at a distance of
417 about 6 m.

418 To mimic the sequential order of fixations and saccades, the grating remained stationary for a
419 fixation period of 533 ms at one of four equally-spaced positions, which we call Position 1 to
420 4, before being shifted rapidly within 67 ms to a new position to start the next cycle of
421 fixation and transition (Fig 1A). In half of the transitions, the shift itself was masked by a gray
422 screen at the mean light intensity of the grating to probe for effects of visual stimulation
423 during the transition. The order of fixation positions and the occurrence of the gray-screen
424 mask were randomized. Altogether, there were 16 possible combinations of grating positions
425 before (“starting position”) and after (“target position”) a transition, and each combination
426 was presented with transitions by grating motion as well as by homogeneous illumination.

427 We observed that ganglion cell responses could depend on both the grating position before
428 and after the transition. Some of the different response patterns and their dependencies on
429 starting and target positions are exemplified by the three sample cells displayed in Fig 1B.
430 Cell 1 responded strongly after transitions from Position 3 to 2 as well as from 1 to 2, but not
431 for transitions from Position 3 to 4, suggesting a preference for a specific target position,
432 namely here Position 2. When comparing firing-rate profiles for transitions via motion and via
433 a gray screen, on the other hand, nearly identical responses were found for each individual
434 combination of starting and target image. This was also the case for the two other sample cells
435 of Fig 1 as well as for the entire population of ganglion cells, except for a small latency effect
436 in some cells (e.g. Cells 2 and 3).

437 For a quantitative comparison of the responses under transitions via motion and via a gray
438 screen, we computed a normalized coefficient of determination R^2 between the two responses
439 (Fig 1D). Most values lay near unity, corresponding to nearly identical response profiles
440 under the two conditions, and values smaller than unity could generally be traced back to
441 relative temporal shifts of the responses. These small differences in response kinetics,
442 however, did not play a role for our analysis of response strength and sensitivity to the pre-
443 and post-saccadic images. We therefore generally pooled responses from motion and gray-
444 screen transitions for further analyses, but also confirmed that the analysis of response types
445 held independently for each of the two transition types (see below).

446 In order to visualize the response characteristics more systematically, we computed the peri-
447 stimulus time histograms (PSTHs) for all 16 combinations of starting and target position and
448 displayed them in a matrix-like fashion (Fig 1C). In this depiction, it becomes immediately
449 apparent that Cell 1 responded strongly when the target grating position was Position 2, but
450 not for other targets, and that the response was only slightly modulated by the starting
451 position. Thus, this cell is sensitive mostly to the post-saccadic image, in this particular case
452 the image that corresponds to the grating at Position 2. Note that the relevant observation here
453 is that there is a preferred target position, not which particular position it is. For the same cell
454 but with a translated receptive field position or for phase-shifted versions of the displayed
455 gratings, the preferred target position might be different, but responses should still primarily
456 depend on which target position was reached.

457 Other ganglion cells, like Cell 2, could display two distinct response peaks, one during the
458 transition itself and one after the onset of the new fixation. For this cell, both peaks occurred
459 when the grating switched from Position 3 to 1, but other sample transitions with a different
460 starting or target position elicited only one or the other (Fig 1B, center). The matrix-like
461 display of all 16 firing rate profiles (Fig 1C, center) reveals that the first peak was sensitive to
462 the starting position, occurring systematically for Positions 2 and 3, whereas the second peak
463 depended on the target position and was elicited by Positions 1 and 4. Note that due to the
464 cyclical nature of the grating, Positions 1 and 4 are neighboring just like Positions 2 and 3 are.

465 For some ganglion cells, responses to the saccadic stimulus depended more intricately on the
466 combination of pre- and post-saccadic images. Cell 3, for example, exhibited increased
467 activity when the grating position changed from 4 to 2, but neither the starting nor the target
468 position alone were sufficient to evoke a strong response if there was no change in the grating
469 position across the transition (Fig 1B, right). Indeed, none of the starting or target positions by

470 itself were sufficient to evoke a response of Cell 3, because starting and target position had to
471 differ to trigger the cell (Fig 1C, right). Thus, this cell was sensitive to a change in the grating
472 position, but invariant to the specific starting and target positions of the transition.

473 In order to systematically compare these response patterns for different types of ganglion
474 cells, we sought a reduced, quantitative description which still captured the dependencies of
475 the responses on the starting position, on the target position, and on whether there was a
476 change of the position. To take the distinct early and late responses of some cells into account
477 (e.g., Cell 2 in Fig 1), we analyzed the peak firing rates in two response windows, the first
478 from 30 ms after transition onset to 10-30 ms (depending on the experiment) after the onset of
479 the new fixation, and the second from 10-30 ms until 200 ms after the onset of the new
480 fixation (Fig 2A).

481 To systematically analyze the dependence of the responses in these two temporal windows on
482 the combination of starting and target position of the grating, we collected the peak firing
483 rates of each window in a 4×4 matrix, corresponding to the 4×4 transitions from starting to
484 target position (Fig 2B). The structure of these two response matrices contains information
485 about the cell's sensitivity to specific grating positions. For example, the first response matrix
486 of Cell 2 from Fig 1, displayed in Fig 2B (left), contains horizontal stripes, demonstrating its
487 sensitivity to specific starting positions (here Positions 2 and 3). The vertical stripes in the
488 response matrix for the second time window (right), on the other hand, correspond to
489 sensitivity to specific target positions.

490 The occurrence of stripes in the response matrices thus denotes the stimulus sensitivity during
491 the selected response window. The specific position of the stripes, however, merely depends
492 on the location of the cell's receptive field relative to the bars of the grating. For example,
493 Position 2 of the grating presumably brought an increase in preferred contrast to the receptive
494 field of Cell 1 in Fig 1, but if that cell's receptive field had been displaced by a quarter grating
495 period in the right direction, the same response peak would have occurred for Position 3
496 instead.

497 Therefore, in order to make the analysis invariant to the receptive field position, we applied a
498 two-dimensional Fourier transformation to the response matrices and only considered the
499 amplitudes of the Fourier components. This yielded a 4×4 matrix for each of the two time
500 windows (Fig 2C). The Fourier component amplitudes in these matrices capture how strongly
501 different wave-like (or stripe-like) patterns are represented in the response matrices, such as

502 stripes along the horizontal, vertical, or diagonal directions. Information about the exact
503 positions of these stripes, on the other hand, is contained in the phases of the Fourier
504 components, which was discarded in our analysis in order to assess the structure of the
505 response matrices independent of relative position (or phase).

506 Three entries of the Fourier transformed response matrices are of particular interest as they
507 correspond to the aforementioned sensitivities to starting position, target position, and change
508 of position (pointed out by arrows in Fig 2C; corresponding insets show a typical response
509 matrix pattern represented by the entry). Simple patterns with single horizontal and vertical
510 stripes in the response matrices, for example, corresponding to sensitivity to the starting and
511 target position, are captured by the (0, 1) and the (1, 0) entry, respectively, of the Fourier
512 transform regardless of the exact preferred position; patterns with diagonal stripes, on the
513 other hand, are typically reflected in the (3, 1) components. These relevant entries are pointed
514 out by arrows in Fig 2C, and corresponding insets show stereotypical response matrix patterns
515 represented by these components.

516 The entries (0, 2), (2, 0), and (2, 2) would correspond to higher harmonics in the sensitivity
517 matrix (e.g., high activity for Position 1 and 3 but low activity for Position 2 and 4), and the
518 (1, 1) component to activity patterns along the other diagonal in the response matrix, from
519 top-left to bottom-right. As expected, such patterns are generally not observed in our data, and
520 the corresponding Fourier components are always near zero. The remaining components
521 either capture the mean activity, namely the (0, 0) component, or are redundant copies of
522 components already discussed. Thus, for each response window, there are three entries of the
523 Fourier transformed response matrices that capture the basic sensitivity pattern of the cell: the
524 (0, 1), the (1, 0), and the (3, 1) components, which correspond to the aforementioned
525 sensitivities to starting position, target position, and change of position.

526 As an example, the cell of Fig 2 exhibited a large (0, 1) Fourier component for the first time
527 window and a large (1, 0) component for the second time window, reflecting its sensitivity to
528 starting and target position in the first and second response window, respectively. Cell 3 from
529 Fig 1, on the other hand, had a diagonal stripe in its second response matrix, reflected by a
530 large (3, 1) entry (data not shown). Note that, in the case of this Cell 3, the large (3, 1) Fourier
531 component was caused by decreased activity along the diagonal of equal starting and target
532 position. On the other hand, since our analysis disregards phase information of the Fourier
533 transform, a large (3, 1) entry could also signify increased activity along this diagonal,
534 corresponding to sensitivity to recurrence of the same grating position across the transition.

535 Such sensitivity to image recurrence has indeed been described for certain ganglion cells of
536 the mouse retina (Krishnamoorthy et al., 2017). For the present datasets from the marmoset,
537 however, we did not find any image-recurrence-sensitive cells. A strong (3, 1) entry in our
538 data always corresponded to a decrease of responses along the diagonal and thus a response
539 sensitivity to a change of the grating position. Finally, for some cells, none of the three entries
540 described above contained a large value. In such a case, the cell either did not respond at all
541 during the corresponding time window or responded indifferently to all transitions with no
542 dependence on the starting or target position or any combination of the two.

543 To compare the sensitivities to pre-saccadic and post-saccadic images and combinations
544 thereof across cells, we combined the three relevant entries of each Fourier transformed
545 response matrix ((0, 1), (1, 0), and (3, 1)) into a three-component vector and normalized it
546 (see Methods). For each response time window, its elements thus characterize a given cell's
547 sensitivity to the starting position, to the target position, and to change in the fixated stimulus
548 pattern across the saccade. Examining this vector for the first response window for each
549 ganglion cell (Fig 2D) shows that this response window was generally only sensitive to the
550 starting position, as the other two Fourier components for target position and change
551 sensitivity were always near zero. This was expected, as the first response occurs too early to
552 be affected by the new fixation and is thus mostly elicited by the offset of the starting position
553 grating. The second response, on the other hand, was dominated by the components
554 corresponding to sensitivity to the target position and to change, with considerable differences
555 in the magnitude of these two components between individual cells, but with generally little
556 sensitivity to the starting position alone (Fig 2E). Thus, this response component is typically
557 affected by the target position of the grating and by combinations of the starting with the
558 target position, consistent with its occurrence several tens of milliseconds after the onset of
559 the new fixation.

560 To jointly analyze the most relevant patterns of stimulus sensitivities during the first and
561 second response window, we thus combined the sensitivity for the starting position of the first
562 response with the target and change sensitivities of the second response to obtain a final three-
563 component vector, which we call the sensitivity vector. The sensitivity vector describes the
564 most pronounced response properties of a ganglion cell under our saccade stimulus (Fig 2F).
565 For example, the sensitivity vector for the sample cell of Fig 2A-C (large yellow dot in Fig
566 2D-F) has large sensitivity values for the starting and the target position, but not for the

567 change of position, reflecting the horizontal and vertical stripes in the response matrices of
568 Fig 2B and the lack of a diagonal structure.

569 As the sensitivity vector provides a general characterization of a cell's sensitivity to pre- and
570 post-transition image information, we used it to re-confirm that there was no significant
571 difference between motion and gray-screen transitions. For each cell, we calculated the
572 sensitivity vector separately for each transition type and assessed their difference as the
573 Euclidean distance between the two sensitivity vectors, normalized by the Euclidean norm of
574 the standard sensitivity vector for the cell. This can be viewed as a relative deviation of the
575 sensitivity profile under motion versus gray-screen transitions, and the small average value of
576 0.16 ± 0.13 (mean \pm standard deviation across all analyzed cells) indicated that sensitivity
577 profiles varied little with transition type. In fact, the relative deviations are consistent with
578 noise, as a corresponding analysis that split the data in half (irrespective of the transition type)
579 yielded comparable relative deviations of the sensitivity vectors of 0.12 ± 0.11 (mean \pm
580 standard deviation), corroborating that the transition type has little influence on the sensitivity
581 profile with respect to pre- and post-transition images.

582 **Responses of Different Cell Classes**

583 We next asked whether the observed differences in response sensitivities were connected to
584 the different types of ganglion cells. To investigate this question, we first classified cells
585 according to standard response characteristics measured under spatiotemporal white-noise
586 stimulation. Specifically, we measured the cells' spatial receptive fields and temporal filters
587 via the spatiotemporal spike-triggered average as well as the cells' output nonlinearities and
588 spike autocorrelations (Fig 3, see Methods for details). Five distinct classes could be readily
589 identified, including the standard types of On and Off parasol as well as midget cells. On and
590 Off parasol cells displayed fast, biphasic temporal filters and extensive receptive field tiling.
591 On and Off midget cells had slower filters and smaller receptive fields. Here, however, tiling
592 could only partially be observed, owing to the limited number of recorded cells. The reason
593 for the unequal sampling of midget and parasol cells likely lies in a recording bias of the
594 multielectrode arrays. The fairly wide spacing of electrodes and likely differences in signal-
595 to-noise ratio of recorded spikes likely results in more misses and rejections during spike
596 sorting for the smaller midget cells. In addition, some midget cells may not have responded
597 well to the applied stimuli, due to their relatively strong receptive-field surround. In addition
598 to these four major primate ganglion cell types, we also identified a fifth type, an Off cell with
599 slow temporal filters and large receptive fields. We here refer to this type as Large Off cells.

600 We found that the identified major cell types exhibited distinct, characteristic responses to the
601 saccadic stimulus. Figure 4 shows representative response profiles, which illustrate the
602 differences in response patterns between the cell types. Many On parasol cells had two
603 separate response components, a first response sensitive to the starting position and a second
604 response sensitive to the target position. For example, the first On parasol cell in Fig 4A (left
605 column, top) displayed an early response peak if the starting position was 4 (weaker if it was
606 1 or 3) and a later response peak if the target position was 2. Other On parasol cells did not
607 show a clear preference for specific starting or target positions and instead responded rather
608 indifferently (Fig 4A, left column, bottom example). The sensitivity vectors of all On parasol
609 cells show that there was a continuum between these two response types with indifferent cells
610 lying closer to the origin (Fig 4B, left column).

611 Fig 4C shows boxplots of the distributions over cells of the different sensitivity components.
612 For On parasol cells (left column), this confirmed that the cells were mostly sensitive to the
613 starting position and (somewhat less) to the target position. Change sensitivity only played a
614 subordinate role. In one experiment, though, we also found a few On parasol cells whose
615 second response did not seem to be sensitive to the target position but rather to the change of
616 position.

617 Similar to On parasol cells, On midget cells (Fig 4A, second column) also showed a first
618 response sensitive to the starting position and a second response sensitive to the target
619 position. In contrast to their parasol counterparts, however, the responses of On midget cells
620 were dominated by the second response peak, which was more pronounced and sustained than
621 the first. This shifts the sensitivity balance towards the target position (Fig 4B, C).

622 For Off parasol cells, the most striking response feature was that many cells were sensitive to
623 a change of the grating position across the transition. This is evident from the reduced
624 responses during the second response window on the diagonal of equal starting and target
625 position in the matrix representation of the PSTHs (Fig 4A, third column) as well as from the
626 large change sensitivity component of the sensitivity vectors (Fig 4B, C). In addition,
627 however, there often was also considerable sensitivity to the specific starting and target
628 positions in the first and second response, respectively.

629 Off midget cells were mainly sensitive to the target position. Both examples in Fig 4A (fourth
630 column) show cells that responded only to the occurrence of one or two specific target
631 positions with only some modulation by the starting position. The moderate amount of

632 modulation by the starting position was such that responses to a recurrence of the same
633 grating position were reduced. This mild change sensitivity is also revealed by the sensitivity
634 vectors (Fig 4B, C). Overall, however, Off midget cell responses were dominated by their
635 target sensitivity, which they displayed more strongly than any of the other cell types.

636 For the Large Off cells, the striking feature was their pronounced sensitivity to the change of
637 the grating position (Fig 4A, right column) with essentially no sensitivity to the specific
638 starting or target position (Fig 4B, C). These cells generally showed no activity during the
639 first response window and transient responses during the second whenever starting and target
640 position differed.

641 There are thus systematic differences in the sensitivity profiles between different cell types as
642 well as some variability within a single type. Given that the spatial structure of the gratings
643 experienced by the cells depend on their receptive fields and that receptive field sizes can
644 differ substantially between cells, we analyzed to what degree this influenced the sensitivity
645 variations within and across cell types (Fig 5). Indeed, for both On parasol cells (Fig 5A, B)
646 and Off parasol cells (Fig 5D, E), we found that the observed variability in starting and target
647 sensitivity depended systematically on receptive field size across our recordings: smaller cells
648 had stronger sensitivity values and larger cells usually responded more indifferently. This
649 makes intuitive sense, as larger receptive fields are more likely to contain both dark and bright
650 bars of the grating for each position. For Off parasol cells, this means that cells with larger
651 receptive fields were typically dominated by their strong sensitivity to the change of the
652 grating position while the specific starting and target positions did not significantly influence
653 the responses (Fig 4A, top example). Smaller Off parasol cells, however, were also sensitive
654 to the actual starting and target positions, which obscured the change sensitivity to some
655 degree (Fig 4A, bottom example).

656 Other aspects of the observed cell-type-specific sensitivity profiles could not be explained by
657 receptive field size. The relatively weak sensitivity to starting position of On midget cells
658 (Fig 5A) as well as Off midget cells (Fig 5D) compared to the cells' target sensitivities
659 (Fig 5B, E), for example, was largely independent of receptive field size and deviated
660 systematically from the start sensitivity of On and Off parasol cells even when receptive field
661 sizes were similar (Fig 5A, D). Moreover, the general weakness of change sensitivity in On
662 cells was independent of receptive field size (Fig 5C), and the three studied types of Off cells
663 each displayed their respective levels of change sensitivity also largely independent of
664 receptive field size (Fig 5F). Note here, that the largest cells, Large Off cells, have the highest

665 change sensitivity and the smallest ones, Off midget cells, the lowest one. Yet, if larger
666 receptive fields directly led to change sensitivity, one would expect substantial positive
667 correlation within the individual cell types. Instead, receptive field size and change sensitivity
668 showed either no or only a weak relationship not sufficient to account for cell-type differences
669 ($p>0.05$ for Off midget and Large Off cells; $R=0.15$, $p=0.046$ for Off parasol cells). We thus
670 conclude that change sensitivity is not simply a consequence of smaller or larger receptive
671 fields, but appears to be an intrinsic cell-type-specific feature. Together, these analyses show
672 that different types of ganglion cells systematically differ in how the combination of pre- and
673 post-saccadic images affect the spiking activity during and after a saccade-like image
674 transition.

675 The cell-type-specific differences in sensitivity to starting versus target position raise the
676 question whether this follows from differences in response strength under stimulus onset
677 versus stimulus offset. For example, a midget cell's relatively stronger sensitivity to the target
678 position might come from stronger activation by the onset of the newly fixated target grating,
679 whereas the offset of the previous grating (starting position) triggers little activity. We
680 therefore compared the responses under the saccadic stimulus with responses to onsets and
681 offsets of gratings. Since our data did not contain responses to gratings flashed individually
682 with the same bar width and positions as in the saccadic stimulus, we instead analyzed the
683 responses to the onset and offset of stimulation with contrast-reversing gratings. These also
684 contained on- and offsets at the very start and end of each reversing sequence, preceded and
685 followed by homogeneous mean-intensity illumination. Thus, for each cell, we averaged
686 responses to the onset and offset of the reversing-grating stimulus over bar widths of $60\ \mu\text{m}$
687 and $120\ \mu\text{m}$, near the $90\ \mu\text{m}$ used for the saccade stimulus, and over different spatial phases.
688 We then compared the relative response strengths under onset versus offset, assessed as the
689 average firing rate in the 200 ms following on- or offset, to the relative sensitivity to the target
690 versus starting position.

691 From the sample cells in Fig 6A, B, only the On parasol responded more strongly to the offset
692 than onset of the grating, which is consistent with its stronger sensitivity to the starting than to
693 the target position. We confirmed this observation by comparing the relative strength of the
694 onset vs. offset response with the relative sensitivity for the target vs. the starting position
695 during the saccadic stimulus for all cells (Fig 6C). On parasol cells generally had stronger
696 offset than onset responses and, consistent with this, had greater sensitivity for the starting as
697 compared to the target position. By contrast, responses of all Off-type cells and of the On

698 midget cells were dominated by grating onset as well as by the sensitivity for the target
699 position compared to sensitivity for the starting position.

700 We also investigated how the onset and offset response strengths of the cells depended on the
701 grating size. The findings suggest qualitative differences between On cells (Fig 6D) and Off
702 cells (Fig 6E). While Off cells responded more strongly to a grating onset than offset almost
703 regardless of the grating size, both On parasol and On midget cells responded more strongly
704 to the offset if the grating was sufficiently fine, but not for coarser gratings with bar widths
705 beyond a few hundred micrometers. Thus, it seems that the relative strength of offset versus
706 onset responses depends on the spatial stimulus structure inside the receptive field for On
707 cells.

708 Note, however, that there are some caveats to these analyses of grating onsets and offsets. In
709 particular, the small number of trials from which onset and offset responses could be gathered
710 and the different adaptation states at onset versus offset of the reversing gratings (Appleby
711 and Manookin, 2019; Yu et al., 2022) contribute to variability. Furthermore, the comparison
712 between responses to the saccade-like grating shifts and to grating onset and offset are
713 complicated by differences in grating size and contrast.

714 **Modeling Responses to the Saccadic Stimulus**

715 Given the relationship between the responses to the saccadic stimulus and the onset and offset
716 responses to gratings, we next asked to what degree the different response patterns under the
717 saccadic stimulus followed directly from how the cells responded to simple steps in light
718 intensity. If this was the case, the saccadic stimulus might simply be considered as a sequence
719 of two step-stimuli whose responses superimpose. Alternatively, the temporal vicinity of
720 fixation offset and onset across a saccade could modify or add response characteristics beyond
721 what is triggered by isolated light flashes. If so, this might hint at circuit mechanisms that are
722 triggered specifically by saccades.

723 As the saccade-like motion transition of the stimulus evoked essentially the same responses as
724 the gray transition (Fig 1), the saccadic stimulus can be understood as a combination of an
725 offset of bright and dark regions followed by an onset of a new bright/dark pattern. We
726 therefore compared the responses to the saccadic stimulus with responses to full-field
727 brightness steps from mean light intensity (gray) to high intensity (white) or to low intensity
728 (black) and back to gray. For this stimulus, all brightness changes are temporally separated by

729 several hundred milliseconds so that they can be considered as individual stimulation events
730 with little influence on each other.

731 Under the full-field brightness steps, as expected, On cells responded to an increase in
732 brightness whereas Off cells responded to a decrease, and parasol cells responded more
733 transiently than midget cells (Fig 7A). The Large Off cells also responded transiently to
734 decreases of the brightness, but with a longer latency than Off parasol cells.

735 To assess the relation between the responses to brightness steps and responses to the saccadic
736 stimulus, we aimed at modeling the latter based on the former (Fig 7B). Since the saccadic
737 stimulus contains spatially structured images and given that ganglion cells can pool signals
738 over space either linearly or nonlinearly (Enroth-Cugell and Robson, 1966; Hochstein and
739 Shapley, 1976; Schwartz and Rieke, 2011; Gollisch, 2013; Turner and Rieke, 2016;
740 Karamanlis and Gollisch, 2021; Zapp et al., 2022), we correspondingly set up two models
741 with either linear or nonlinear spatial integration. The two models only differed in the order of
742 two simple operations: averaging signals across the receptive field and turning light-intensity
743 steps into firing rate via the measured responses to full-field brightness steps. In the spatially
744 linear model, light intensity values of the gratings are first averaged over the receptive field,
745 and this averaged signal is used to select and scale the appropriate responses to full-field
746 brightness steps to obtain response predictions at fixation offset and at the subsequent new
747 onset.

748 The spatially nonlinear model, on the other hand, first treats every stimulus pixel
749 independently to select the appropriate responses to full-field brightness steps according to the
750 pixel's brightness changes in the saccade stimulus. These pixel contributions are then
751 averaged across the receptive field. This averaging of the brightness-step responses
752 incorporates local nonlinearities because—unlike in the spatially linear model—the
753 contributions of pixels with opposite contrast do not cancel each other out. For example, the
754 spatially nonlinear model responds to gratings even when brightening and darkening inside
755 the receptive field are perfectly balanced because the brightness-step responses to preferred
756 and non-preferred contrast changes are typically non-symmetric and therefore do not cancel.
757 Thus, while the linear model predicts responses only according to the average brightness
758 changes in the receptive field, the nonlinear model also includes the spatial structure of a
759 stimulus in its response.

760 Note that computing the firing-rate contributions on the level of individual pixels (less than
761 $10\ \mu\text{m}$ for our display) may seem counterintuitive, as this is far below the scale of bipolar cell
762 receptive fields (Dacey et al., 2000), which are thought to correspond to the nonlinear
763 subunits of ganglion cell receptive fields and thereby give rise to spatial nonlinearities (Demb
764 et al., 2001; Borghuis et al., 2013; Turner and Rieke, 2016; Yu et al., 2022). Yet, because the
765 stripes of the applied grating with a width of $90\ \mu\text{m}$ are much broader than the individual
766 pixels and also similar in size or larger than expected subunits, the use of individual pixels is
767 essentially identical to using larger subunits. For most subunits, most of the pixels experience
768 the same sequence of light intensities and therefore contribute identical response profiles to
769 the ganglion cell's firing rate. For the applied grating stimulus, treating each pixel
770 individually is thus a good approximation while avoiding the need to specify a particular
771 subunit layout. Note also that the nonlinear model does not contain a second nonlinear step
772 that would account for overall response transformations after spatial integration. Limiting the
773 model to a single nonlinear stage was done for simplicity, so as to evade any parameter fits,
774 and for keeping the complexity of the linear and the nonlinear model identical.

775 For both the linear and the nonlinear model, the receptive field was obtained by separating the
776 spike-triggered average from spatiotemporal white-noise stimulation (Chichilnisky, 2001)
777 into a spatial and a temporal component and fitting a two-dimensional Gaussian to the latter.
778 For each of the 16 transitions in the saccade stimulus, predictions were first assembled
779 separately for the offset of the previously fixated grating and the onset of the new grating
780 before summing the two contributions with a relative delay that corresponded to the transition
781 time. The only two free parameters in the models were an overall scaling of response
782 amplitude and an overall temporal shift of the predictions, which accounted for amplitude and
783 latency differences due to differences in applied contrast. The amplitude scaling, however, did
784 not affect our Fourier-based analysis.

785 For On cells, we found that the responses to the saccadic stimulus could generally be
786 predicted well by at least one of the two models. The responses of On parasol cells were
787 captured well by the nonlinear model, but not by the linear model. The linear model failed, for
788 example, to recreate the strong responses of the sample On parasol cell of Fig 8A (left) to
789 transitions between Positions 2 and 4 (Fig 8B). These grating positions yielded roughly equal
790 bright and dark contrast in the cell's receptive field (Fig 8D), and the linear model therefore
791 predicted no response, because these regions could cancel each other out. By contrast, the
792 nonlinear model correctly captured the response patterns (Fig 8C). It also succeeded in

793 predicting a first response sensitive to the starting position and a second response sensitive to
794 the target position, even though it underestimated the strength of modulation of the second
795 response caused by the target position.

796 In order to quantify the accuracy of the model predictions, we computed modified coefficients
797 of determination R^2 between the response matrices of the experimental data of a cell and the
798 response matrices as calculated from the modeled PSTHs (see Methods). For each response
799 window, this yielded one value per cell and model, which usually lay in the range of zero (no
800 correlation between model and data in that response window) to unity (perfect correlation
801 between model and data). For the On parasol cells, the nonlinear model, but not the linear
802 model, generally achieved R^2 values close to unity, especially for the first response window
803 and only slightly less so for the second response window (Fig 8E), corroborating the spatial
804 nonlinearity of On parasol receptive fields under these stimulus conditions.

805 While the computed coefficients of determination quantify how well the amplitudes of the
806 response peaks in the PSTHs are captured, they do not directly assess whether the models
807 capture a cell's sensitivity characteristics with respect to starting position, target position, and
808 change of the grating. As an alternative measure of model accuracy, we therefore computed
809 the distance between the measured sensitivity vector of a cell and the sensitivity vector
810 calculated from the modeled responses. A small distance indicates that the response
811 sensitivities have been reproduced, while a large distance represents discrepant sensitivities.
812 For the On parasol cells, the distance of the linear model's sensitivity vectors to the
813 experimental sensitivity vectors was generally large, while the nonlinear model produced
814 small distances (Fig 8F). This confirms that On parasol responses to the saccadic stimulus
815 could be modeled well by using the responses to a full-field stimulus and assuming a
816 nonlinear receptive field. Only in one experiment, a subset of On parasol cells with unusually
817 slow and weak responses to the full-field brightness step from black to gray were not modeled
818 well by the nonlinear model.

819 On midgrid cells, like the example in Fig 8A-C (right), were modeled decently by both the
820 linear as well as the nonlinear model. Here, the linear and the nonlinear model yielded similar
821 response predictions because the small receptive fields of these cells contained mostly only a
822 single bar of the grating (Fig 8D). Due to the lack of spatial structure within the receptive
823 field, the spatial nonlinearity played hardly any role. While the strength of the sample cell's
824 second response was partially overestimated, the main response properties, i.e. the transient,
825 start-sensitive first response and the sustained, target-sensitive second response, were

826 successfully predicted. For both response windows, the models achieved relatively high R^2
827 measures of the response matrices, with a tendency towards better predictions by the
828 nonlinear model (Fig 8E; $p=2.1\times 10^{-5}$ and $p=3.3\times 10^{-6}$ for first and second window,
829 respectively, Wilcoxon signed-rank test). The distance of sensitivity vectors, on the other
830 hand, did not show a clear trend (Fig 8F; $p=0.21$, Wilcoxon signed-rank test).

831 In contrast to On cells, the responses of Off parasol as well as Large Off cells could only
832 partially be explained by the linear or nonlinear model. The linear model displayed similar
833 problems for Off parasol and Large Off cells as it did for On parasol cells, often strongly
834 underestimating the responses (e.g. Fig 9B) due to cancelation that does not occur in the
835 nonlinear receptive fields of these cells. By contrast, the nonlinear model could mostly
836 reproduce the sensitivities to the starting and target position (Fig 9C). However, the responses
837 on the diagonal, i.e., to a recurrence of the grating position, were consistently overestimated.
838 For example, the Off parasol cell of Fig 9 lacked a strong second response to the transition
839 when starting and target position were both Position 4. Both models predicted such a
840 response, since the receptive field returned to being mostly filled with black after the
841 transition (Fig 9D). Accordingly, both the similarity between response matrices (Fig 9E) and
842 the sensitivity vector distance (Fig 9F) show that the models did not capture the response
843 characteristics of Off parasol and Large Off cells as successfully as for other cell types.

844 For Off midgrid cells, akin to On midgrid cells, the small size of their receptive fields led to
845 similar predictions by the linear and nonlinear model (Fig 9A-D, middle column). For the
846 sample Off midgrid cell, the general target sensitivity was reproduced, although responses to
847 Position 4 as target position were overestimated, possibly a result of noise in the receptive-
848 field measurement. Furthermore, the slight modulation of the responses by the starting
849 position, hinting at some change sensitivity, was not captured by the models. For the first
850 response window, the models achieved comparatively low R^2 values (Fig 9E), largely because
851 Off midgrid cells responded only weakly and unreliably during this window. For the second
852 response window, however, which included the bulk of the Off midgrid responses, both
853 models achieved decent R^2 values, but were likely suffering somewhat from the mild change
854 sensitivity in the responses that was not captured by the models. The distance between the
855 modeled and measured sensitivity vectors of the Off midgrid population was rather small
856 (Fig 9F), indicating that the general sensitivity profiles of Off midgrid cells could mostly be
857 explained by their responses to the full-field brightness steps.

858 The analysis of Fig 5 had shown us that the receptive field size appears to directly influence
859 some of the assessed sensitivities under our saccadic stimulus. We therefore used the obtained
860 models to evaluate in simulations how the receptive field size affected the distinct response
861 characteristics. To do so, we evaluated the response predictions by the models for each cell,
862 with receptive fields scaled to a range of different sizes, and analyzed the resulting
863 sensitivities, averaged over all cells of a particular type.

864 The sensitivities of the linear model's predictions were independent of the receptive field size
865 (Fig 10, dashed lines). While the model produced weaker responses for larger receptive fields,
866 owing to increasing cancelation from bright and dark regions inside the receptive field, the
867 relative differences in average brightness levels of different grating positions remained and
868 thus the preference for certain starting and target positions. In a more realistic setting, of
869 course, the increasingly weak responses would be overshadowed by noise, thereby reducing
870 all sensitivities.

871 The nonlinear model, on the other hand, directly predicted decreasing sensitivities for starting
872 and target position with increasing receptive field size (Fig 10, solid lines), as the responses
873 became more indifferent to them. This characteristic qualitatively matched our observations
874 for different cell types, most notably for On and Off parasol cells. Yet, the predicted curves do
875 not always quantitatively align with the data, and the general declining shape of all curves
876 does not capture the fact that parasol cells, despite their larger receptive fields, were more
877 sensitive to the starting position than midget cells. Thus, although receptive field size clearly
878 shapes the cells' sensitivities to starting and target position, it alone cannot explain the cell-
879 specific preferences for starting or target position. It seems likely that, instead, the faster
880 response kinetics of parasol cells and the strong preference of On parasol cells for offsets
881 compared to onsets of gratings (Fig 6) play the larger role here. Moreover, the unexplained
882 sensitivity to change across the transition, as observed mostly for Off cells, was not predicted
883 by any of the tested receptive field sizes (Fig 10C, F).

884 Figure 11A-C summarizes the sensitivity measures extracted from the two models as well as
885 from the data. Evidently, while the sensitivity to starting and target position could generally
886 be explained by a cell's preference for light increments and decrements (Fig 11A, B), in
887 particular when using the nonlinear model, the change sensitivity could not (Fig 11C).
888 Accordingly, the sensitivity vectors that were calculated from the model responses were
889 largely restricted to the plane spanned by starting and target sensitivity; the predicted change
890 sensitivity was always close to zero (Fig 11D, E). Therefore, the measured change sensitivity

891 of Off parasol and Large Off cells and potentially also of Off midget cells appears to be the
892 result of additional mechanisms. These mechanisms have the effect of spreading out the
893 sensitivity vectors in the analyzed three-dimensional sensitivity space (Fig 11F), thus
894 diversifying the response characteristics of the different cell types under saccade-like image
895 shifts.

896 **Discussion**

897 Saccades pose a unique challenge to the visual system by presenting a rapid transition
898 between two fixated images, separated by only about a hundred milliseconds or less. Despite
899 their ubiquity in nearly all visual animals (Land, 1999), surprisingly little is known about how
900 neurons in the visual system combine information from the pre- and post-saccadic images and
901 what aspects of the two images are encoded in their responses in this context. In the present
902 work, we have shown that responses of ganglion cells in the marmoset retina under saccadic
903 stimulation do not simply represent the new fixation, but display a range of different
904 dependencies on both the pre- and post-saccadic image (Fig 1). Quantifying the sensitivity to
905 the starting position, the target position, and change across the transition (Fig 2) revealed that
906 different ganglion cell types systematically displayed different sensitivity patterns (Figs 3-5)
907 and that some of those patterns can be related to their responses to individually flashed pre-
908 and post-saccadic images (Fig 6). Using simple models with linear and nonlinear stimulus
909 integration over space (Fig 7) showed that the dominant sensitivities of parasol and midget On
910 cells could be reproduced based on the cell's responses to isolated flashes of light intensity
911 (Fig 8). By contrast, for many Off cells, especially Off parasol and a class of Large Off cells,
912 the models failed to account for the observed sensitivity to change across the transition
913 (Figs 9 and 10). Thus, the Off cells' change sensitivity appears to require more complex
914 circuit mechanisms, which are not triggered under isolated light-intensity flashes. This entails
915 a new asymmetry in the functional properties of On and Off ganglion cell classes and
916 contributes to diversifying the response patterns to saccade-like image transitions (Fig 11).

917 **Retinal Coding of Image Shifts**

918 In search of the origins of saccadic suppression, multiple studies in various non-primate
919 vertebrates have looked at the influence of saccades on the response strength of ganglion cells
920 and found a diverse picture of enhancement, suppression, and indifference (Roska and
921 Werblin, 2003; Amthor et al., 2005; Sivyer et al., 2019; Idrees et al., 2020). Fewer studies

922 have investigated what ganglion cells encode during or after saccades, despite the likely
923 importance of fixation onset for eliciting informative responses (Segev et al., 2007).
924 Moreover, saccade-like image shifts may alter the message conveyed by ganglion cell spikes,
925 as observed in the salamander retina, where On-Off ganglion cells were found to transiently
926 switch their relative sensitivity to On-type versus Off-type stimuli after an image shift (Geffen
927 et al., 2007). In an early study in the cat, Noda and Adey (1974) found sustained cells
928 (probably X-cells) that responded to preferred contrast in the target image, and transient cells
929 (probably Y-cells) that signaled the occurrence of a saccade. This is reminiscent of our
930 findings of Off midget cells dominated by their target sensitivity and On parasol cells with
931 large receptive fields that responded indifferently.

932 In a previous study from our lab, we had identified ganglion cells in the mouse retina that
933 responded distinctly to the recurrence of an image (Krishnamoorthy et al., 2017). In the
934 present study of the marmoset retina, we did not find such image-recurrence-sensitive cells
935 among the investigated types. Cells with distinct responses to recurring images (Off parasol
936 and Large Off cells) displayed decreased responses for these transitions and thus sensitivity to
937 change rather than image recurrence. Although we cannot exclude that the primate retina also
938 has ganglion cells with sensitivity to image recurrence, this might also reflect a divergence
939 between mouse and primate ganglion cell types (Peng et al., 2019), demonstrating the
940 different visual requirements of these species (Baden et al., 2020).

941 **Relation of sensitivity profiles to basic response characteristics**

942 Our data showed that different cell types have different relative sensitivities to the offset of
943 the pre-saccadic and the onset of the post-saccadic image, as measured by the start and target
944 sensitivity, respectively. These cell-type differences seem to mostly follow the characteristics
945 of responses to simple flash stimuli, such as temporally isolated onsets and offsets of gratings.
946 Cell types with particularly strong responses to grating offsets, like On parasol cells, also
947 display the highest sensitivity to the starting position, whereas cells with relatively weak
948 grating offset responses, like Off midget cells, were rather sensitive to the target position
949 (Figure 6). Furthermore, these sensitivities were approximately reproduced by computational
950 models that were based on how the cells responded to step-like changes in light intensity
951 (Figure 11A-B). By contrast, the cell-type differences in change sensitivity are an aspect that
952 does not follow from simple response characteristics, as illustrated both by the finding that
953 change sensitivity does not critically depend on receptive field size (Figures 5F & 10F) and

954 by the failure of the flash-response-based models to reproduce change sensitivity (e.g.,
955 Figure 11C).

956 **Large Off Cells**

957 In addition to the standard midget and parasol ganglion cells, we also identified a fifth cell
958 type, which we called Large Off cells. We distinguished these cells from Off parasol cells
959 because they had slower temporal filters, larger receptive fields, and did not match Off
960 parasol tiling. The identity of these cells is unknown, but the similarity of their response to
961 Off parasol cells could suggest that they might be Off smooth monostratified (Off SM)
962 ganglion cells, though other candidates, e.g., Off narrow thorny ganglion cells, also exist
963 (Dacey, 2004; Masri et al., 2019; Grünert and Martin, 2021). In the macaque retina, Off SM
964 cells have been described as similar to Off parasol cells, but with a longer latency and larger
965 receptive fields (Crook et al., 2008). In addition, SM cells tend to have irregular receptive
966 fields with a hotspot structure (Rhoades et al., 2019), matching our observation that the Large
967 Off cells in our recordings had more irregular receptive fields than parasol cells. Yet, we did
968 not find the counterpart of the Off SM cells, the On SM cells, and the difference in receptive
969 field size between Large Off and Off parasol cells was smaller than what would have been
970 expected from Off SM cells in the macaque retina (Crook et al., 2008; Rhoades et al., 2019).
971 The latter, however, might be a species-specific difference between macaque and marmoset or
972 might result from differences in retinal eccentricity.

973 **Potential Mechanisms Underlying Responses to Saccadic Stimulation**

974 The model analysis showed that the sensitivity to the starting and target position could largely
975 be explained by a cell's responses to full-field brightness steps, at least when nonlinear spatial
976 integration is accounted for. Some differences between the cell types seem to follow from
977 differences in response kinetics. The fast responses of the On parasol cells, for example, allow
978 for a strong and distinct response to the onset of the transition with corresponding pronounced
979 start sensitivity, whereas the slower Off midget cells respond mostly only after the new
980 fixation has started and are thus more sensitive to the target position.

981 Less clear is what the mechanism behind the change sensitivity observed in Off cells, in
982 particular Off parasol and Large Off cells, might be. One hypothesis could be that transitions
983 with no net change in the image pattern are simply too brief to be detected by the temporal
984 filters of the ganglion cells, in particular since we did not observe different responses for
985 motion and gray transitions. For Off midget cells, this could potentially be a sufficient

986 explanation, since these cells generally have slow temporal filters and their change sensitivity
987 is only mild. For Off parasol cells, however, the temporal filters that we extracted from the
988 spike-triggered average typically peaked far before 67 ms, which is the duration of the
989 transition, and the change sensitivity of Large Off cells appears too stark to be caused simply
990 by slow temporal filtering. In addition, distinct responses to the onset as well as the offset of
991 the transition are visible for all analyzed cell types except Off midget cells. Therefore, it
992 seems unlikely that temporal filtering is so slow as to cause change sensitivity.

993 Alternatively, neuronal or synaptic fatigue of local excitatory inputs accrued during the
994 fixation of several hundred milliseconds prior to the transition might prevent responses to the
995 new fixation when the same image recurs. However, the pronounced transiency of responses
996 in Off parasol and Large Off cells and the lack of sustained activity speak against strong
997 presynaptic activity that could trigger the required fatigue, which would need to be strong
998 enough, for example, to prevent any response to recurring grating positions in Large Off cells.

999 Instead, we hypothesize that change sensitivity is caused by inhibition and propose a
1000 mechanism of local delayed crossover inhibition. In this mechanism, the Off bipolar cells that
1001 provide excitatory input to the change-sensitive Off cells receive inhibitory input (presumably
1002 onto their axon terminals) from slow, narrow-field On-type amacrine cells. For recurring
1003 grating positions, this means that the local excitation from the dark stripes of the grating at the
1004 onset of the new fixation will be suppressed by inhibition that was triggered by the
1005 brightening at the same locations when the pre-saccadic grating disappeared. This previously
1006 triggered inhibition will not yet have decayed, if the activity of the corresponding amacrine
1007 cell is sustained enough to last across the duration of the transition.

1008 Crossover inhibition is the dominant inhibitory input to parasol cells and serves various
1009 functions by shaping ganglion cell responses in many species (Manookin et al., 2008;
1010 Werblin, 2010; Crook et al., 2011; Cafaro and Rieke, 2013; Rosa et al., 2016). For our
1011 hypothesized mechanism, however, we consider crossover inhibition that acts presynaptically,
1012 that is, onto bipolar cell terminals, and thereby shapes the excitatory input received by the
1013 parasol cells. This presynaptic component of crossover inhibition would act locally,
1014 suppressing only the input from certain bipolar cell locations, as required for our hypothesized
1015 mechanism of change sensitivity. Such presynaptic crossover inhibition has indeed been
1016 observed for parasol cells in the macaque retina (Crook et al., 2014; Manookin et al., 2018),
1017 as well as in other systems, such as the rabbit retina (Wässle and Boycott, 1991; Molnar and
1018 Werblin, 2007). This inhibition seems to be glycinergic (Crook et al., 2014), making

1019 glycinergic narrow-field amacrine cells with their comparatively small receptive fields
1020 (Pourcho and Goebel, 1985; Menger et al., 1998; Masland, 2012) the likely candidate source.
1021 In cat, rabbit, and rat retina, for example, the narrow-field AII amacrine cell receives On input
1022 from bipolar cells and provides glycinergic inhibition to Off bipolar axon terminals (Kolb and
1023 Famiglietti, 1974; Demb and Singer, 2012), and a similar circuitry is also present in the
1024 macaque retina (Wässle et al., 1995).

1025 The fact that Off parasol cells display change sensitivity, but On parasol cells do not, might
1026 then suggest that there are differences in the presynaptic crossover inhibition between these
1027 cells types. Little detail is known about these interactions, yet differences do exist. For
1028 example, blocking presynaptic inhibition unmasks a strong excitatory Off input to On parasol
1029 cells, which is not matched by corresponding inputs to Off parasol cells (Crook et al., 2014;
1030 Manookin et al., 2018). With respect to change sensitivity, one hypothesis might be that the
1031 functionally relevant difference of the presynaptic crossover inhibition lies in its timing. At
1032 the postsynaptic level of input to the ganglion cells, for example, crossover inhibition under
1033 reversing gratings is delayed with respect to excitation in Off, but not in On parasol cells
1034 (Crook et al., 2014). If a similar timing relation occurs at the presynaptic level, the crossover
1035 inhibition from the offset of the previous fixation could be delayed enough for Off, but not On
1036 parasol cells, to act on the onset of the new fixation and thereby suppress excitation at
1037 locations where preferred contrast recurs across the transition. When no part of the receptive
1038 field has a net increase in preferred contrast across the transition, responses of Off parasol
1039 cells would thus be diminished, whereas On cells could still respond, as the presynaptic
1040 inhibition may have already sufficiently decayed for these cells.

1041 With respect to excitatory inputs to the ganglion cells, our efforts to model responses to the
1042 saccadic stimulus showed that spatial nonlinearities within the receptive field need to be
1043 accounted for in several cell types, in particular parasol and the Large Off cells. Rectified
1044 input from bipolar cells is the prime candidate for this (Demb et al., 2001; Borghuis et al.,
1045 2013; Turner and Rieke, 2016; Yu et al., 2022). Other mechanisms likely also contribute to
1046 shaping the responses. Gap-junction coupling between bipolar cells may alter the scale of
1047 spatial nonlinearities (Kuo et al., 2016). Moreover, these gap junctions have been shown to
1048 mediate motion sensitivity in macaque parasol ganglion cells (Manookin et al., 2018; Appleby
1049 and Manookin, 2020; Liu et al., 2021) and may thus similarly modulate responses to the rapid
1050 temporal image sequence across a saccade.

1051 Inhibition from the receptive-field surround should also be triggered by the saccadic stimulus,
1052 since the gratings span the entire retina piece in the experiment, much beyond individual
1053 receptive-field centers. Yet, for parasol cells, despite their spatially nonlinear receptive-field
1054 center, surround suppression appears mostly mediated by horizontal cells (McMahon et al.,
1055 2004; Davenport et al., 2008), which likely do not respond strongly to the applied fine
1056 gratings because of their linear response characteristics. Moreover, given the spatial extent of
1057 the receptive-field surround, it seems likely that surround suppression is similar for each of
1058 the four grating positions and therefore does not contribute to sensitivity for a particular
1059 starting or target position. Yet, in principle, surround suppression could contribute to the
1060 sensitivity to change if there are sufficiently small nonlinear subunits in the surround
1061 (Takeshita and Gollisch, 2014) or surround inhibition acting directly on bipolar cell subunits
1062 (Protti et al., 2014). Adaptation in surround subunits, however, would rather decrease change
1063 sensitivity, as inhibition should be reduced for a recurring grating position, and thus does not
1064 present a likely mechanism for change sensitivity. Yet, future experiments might attempt to
1065 directly test for surround contributions by restricting the grating presentation to small spatial
1066 regions.

1067 **Limitations and Future Directions**

1068 The stimulus used here differs from real saccades in two important aspects. Firstly, the
1069 transition is not a real motion stimulus due to the limited framerate of our projection system.
1070 Yet, the high speed of a saccade and the corresponding motion blur make it likely that true
1071 saccadic motion and homogeneous illumination at mean light level are nearly equivalent
1072 stimuli for the retina, and we therefore do not expect this to strongly influence the findings
1073 regarding the encoding of pre- and post-saccadic images. Secondly, the applied gratings are
1074 artificial patterns, whose activation of the retinal circuitry may differ from that of natural
1075 stimuli (Turner and Rieke, 2016; Yu et al., 2022), though analyses of macaque ganglion cell
1076 responses to natural scenes containing self-motion signals found good correspondence of
1077 response characteristics with those typically obtained with simpler, artificial stimuli
1078 (Schottdorf and Lee, 2021). For the present work, the periodic nature of the gratings proved
1079 useful in allowing us to apply Fourier analysis for systematically analyzing the sensitivity
1080 profile of each cell independent of the particular position of a cell's receptive field. This may
1081 pave the way for future investigations of responses to saccades with natural images.

1082 The use of gratings with only a single spatial scale in our recordings may raise the question
1083 whether the analyzed sensitivity patterns differ for different spatial scales and whether some

1084 of the cell-type differences follow from differences in receptive field size between the types.
1085 The analysis of how sensitivities depend on receptive field size within cell types (Figure 5)
1086 provides at least a partial answer. Taking advantage of the fact that receptive field sizes for
1087 individual cell types varied by about a factor of two across our data, we found that the cell-
1088 type specificity of change sensitivity, for example, did not follow from differences in
1089 receptive field size. Moreover, the different types of Off cells displayed different change
1090 sensitivity even when cells of similar sizes were compared. Likewise, On midget and parasol
1091 cells differed in their start sensitivity independent of receptive field size. Nonetheless, future
1092 variations of the stimulus, including gratings with a smaller or larger spatial frequency, would
1093 be useful to study the generality of our findings. For example, probing the small midget cells
1094 with stimuli that contain substantial spatial structure in their receptive fields might elucidate
1095 whether Off midget cells robustly display some level of change sensitivity or whether their
1096 responses simply deteriorate at higher spatial frequency.

1097 Regarding our analysis approach, we note that the response patterns elicited by the saccadic
1098 stimulus could contain additional structure that is not captured by our separation into two
1099 response windows and analysis of peak firing rates. The two applied response windows make
1100 intuitive sense, however, as they relate to the offset and onset of fixated images, and many
1101 cells indeed displayed distinct response peaks in the two time windows, in particular On
1102 parasol cells, but also Off parasol and On midget cells. As these peaks were similar in timing
1103 across types within a given piece of retina, it allowed us to use a single boundary to separate
1104 these response components. For Off midget cells, this separation is less clear, as responses
1105 were more sustained without distinct peaks and only little activity in the first response
1106 window. Thus, one might ask whether a potential offset response might come later and
1107 overlap with the subsequent onset response.

1108 But Off midget cells generally did not show any sizeable offset-triggered response that would
1109 be invariant to the target position (c.f. the two sample Off midget cells of Figure 4, in
1110 particular for the 2-to-2 transition in the top row and the 4-to-4 transition below, which both
1111 have the preferred starting position). Thus, responses of Off midget cells are not consistent
1112 with containing a strong offset-specific (and target-invariant) response component that would
1113 be mixed with the onset component; instead, the particular starting position can modulate the
1114 response that is triggered by the preferred target position, which is what is captured in our
1115 analysis as change sensitivity.

1116 Future experiments might probe the time scales of the response components and their
1117 interactions further by varying the duration of the transition period. This might help reveal,
1118 for example, the timescale of the change sensitivity and relate this to potential inhibitory
1119 mechanisms. Finally, to test if crossover inhibition is involved in generating the change-
1120 sensitive responses of Off cells, blocking the On pathway with L-AP4 (Slaughter and Miller,
1121 1981) could be applied to remove On-type inhibition, even though this would not reveal
1122 specifics of the potential crossover circuitry.

1123 **Asymmetry of the On and Off Pathways**

1124 The On and Off pathways in the retina had originally been viewed as symmetric, i.e.,
1125 exhibiting the same response properties but for light increments and decrements, respectively
1126 (Schiller, 1992). Later, however, several studies found asymmetries between the On and Off
1127 pathways, such as differences in the spatiotemporal receptive field properties of macaque On
1128 and Off parasol ganglion cells (Chichilnisky and Kalmar, 2002). These differences might be
1129 linked to different connectivity in the underlying circuitry of the On and Off pathways found
1130 in primates and other species (Molnar and Werblin, 2007; Khuc-Trong and Rieke, 2008) and
1131 to the more strongly rectified synaptic input received by primate Off parasol cells, but also,
1132 e.g., guinea pig Off Y-cells, compared to their On counterparts (Zaghloul et al., 2003; Turner
1133 and Rieke, 2016). Importantly, these asymmetries extend to relevant functional differences
1134 like the encoding of natural images (Turner and Rieke, 2016).

1135 While asymmetries between On and Off parasol cells (or Y-cells in other species) have been
1136 described previously, the midget pathways have received less attention. In the present work,
1137 we found asymmetries between the On and Off pathways of both parasol as well as midget
1138 ganglion cells. While Off midget cells were strongly sensitive to the target image with some
1139 change sensitivity, On midget cells were not change-sensitive, but responded transiently to the
1140 preferred starting image. The asymmetric responses of parasol cells were even more striking.
1141 While On parasol responses represented images before and after a transition successively, Off
1142 parasol cells performed a computation across the transition by responding specifically to a
1143 change of the image. The different response characteristics suggest that On and Off cells
1144 encode different features of the visual stimulus in the context of saccades, similar to recent
1145 suggestions about the functional benefit of differences in spatial integration between On and
1146 Off parasol cells (Yu et al., 2022). This may allow the joint activity patterns of On and Off
1147 pathways to cover a more versatile stimulus space at the onset of a new fixation than
1148 pathways with similar sensitivity profiles, but opposing contrast sensitivity.

1149 **Bibliography**

- 1150 Amthor FR, Tootle JS, Gawne TJ (2005) Retinal ganglion cell coding in simulated active
1151 vision. *Vis Neurosci* 22:789–806.
- 1152 Appleby TR, Manookin MB (2019) Neural sensitization improves encoding fidelity in the
1153 primate retina. *Nat Commun* 10:4017.
- 1154 Appleby TR, Manookin MB (2020) Selectivity to approaching motion in retinal inputs to the
1155 dorsal visual pathway. *eLife* 9:e51144.
- 1156 Baden T, Euler T, Berens P (2020) Understanding the retinal basis of vision across species.
1157 *Nat Rev Neurosci* 21:5–20.
- 1158 Borghuis BG, Marvin JS, Looger LL, Demb JB (2013) Two-Photon Imaging of Nonlinear
1159 Glutamate Release Dynamics at Bipolar Cell Synapses in the Mouse Retina. *J*
1160 *Neurosci* 33:10972–10985.
- 1161 Cafaro J, Rieke F (2013) Regulation of Spatial Selectivity by Crossover Inhibition. *J Neurosci*
1162 33:6310–6320.
- 1163 Chichilnisky EJ (2001) A simple white noise analysis of neuronal light responses. *Netw*
1164 *Comput Neural Syst* 12:199–213.
- 1165 Chichilnisky EJ, Kalmar RS (2002) Functional Asymmetries in ON and OFF Ganglion Cells
1166 of Primate Retina. *J Neurosci* 22:2737–2747.
- 1167 Crook JD, Manookin MB, Packer OS, Dacey DM (2011) Horizontal Cell Feedback without
1168 Cone Type-Selective Inhibition Mediates “Red–Green” Color Opponency in Midget
1169 Ganglion Cells of the Primate Retina. *J Neurosci* 31:1762–1772.
- 1170 Crook JD, Packer OS, Dacey DM (2014) A synaptic signature for ON- and OFF-center
1171 parasol ganglion cells of the primate retina. *Vis Neurosci* 31:57–84.
- 1172 Crook JD, Peterson BB, Packer OS, Robinson FR, Gamlin PD, Troy JB, Dacey DM (2008)
1173 The Smooth Monostratified Ganglion Cell: Evidence for Spatial Diversity in the Y-
1174 Cell Pathway to the Lateral Geniculate Nucleus and Superior Colliculus in the
1175 Macaque Monkey. *J Neurosci* 28:12654–12671.
- 1176 Dacey D, Packer OS, Diller L, Brainard D, Peterson B, Lee B (2000) Center surround
1177 receptive field structure of cone bipolar cells in primate retina. *Vision Res* 40:1801–
1178 1811.
- 1179 Dacey DM (2004) Origins of perception: retinal ganglion cell diversity and the creation of
1180 parallel visual pathways. In: *The Cognitive Neurosciences* (Gazzaniga MS, ed), pp
1181 281–301. Cambridge, MA: MIT Press.
- 1182 Davenport CM, Detwiler PB, Dacey DM (2008) Effects of pH Buffering on Horizontal and
1183 Ganglion Cell Light Responses in Primate Retina: Evidence for the Proton Hypothesis
1184 of Surround Formation. *J Neurosci* 28:456–464.

- 1185 Demb JB, Singer JH (2012) Intrinsic properties and functional circuitry of the AII amacrine
1186 cell. *Vis Neurosci* 29:51–60.
- 1187 Demb JB, Zaghoul K, Haarsma L, Sterling P (2001) Bipolar Cells Contribute to Nonlinear
1188 Spatial Summation in the Brisk-Transient (Y) Ganglion Cell in Mammalian Retina. *J*
1189 *Neurosci* 21:7447–7454.
- 1190 Enroth-Cugell C, Robson JG (1966) The contrast sensitivity of retinal ganglion cells of the
1191 cat. *J Physiol* 187:517–552.
- 1192 Field GD, Sher A, Gauthier JL, Greschner M, Shlens J, Litke AM, Chichilnisky EJ (2007)
1193 Spatial Properties and Functional Organization of Small Bistratified Ganglion Cells in
1194 Primate Retina. *J Neurosci* 27:13261–13272.
- 1195 Gaveau V, Martin O, Prablanc C, Pélisson D, Urquizar C, Desmurget M (2003) On-line
1196 modification of saccadic eye movements by retinal signals. *NeuroReport* 14:875–878.
- 1197 Geffen MN, de Vries SEJ, Meister M (2007) Retinal Ganglion Cells Can Rapidly Change
1198 Polarity from Off to On. *PLoS Biol* 5:e65.
- 1199 Gollisch T (2013) Features and functions of nonlinear spatial integration by retinal ganglion
1200 cells. *J Physiol-Paris* 107:338–348.
- 1201 Gomes FL, Silveira LCL, Saito CA, Yamada ES (2005) Density, proportion, and dendritic
1202 coverage of retinal ganglion cells of the common marmoset (*Callithrix jacchus*
1203 *jacchus*). *Braz J Med Biol Res* 38:915–924.
- 1204 Grünert U, Martin PR (2021) Morphology, Molecular Characterization, and Connections of
1205 Ganglion Cells in Primate Retina. *Annu Rev Vis Sci* 7:73–103.
- 1206 Hartline HK (1938) The response of single optic nerve fibers of the vertebrate eye to
1207 illumination of the retina. *Am J Physiol* 121:400–415.
- 1208 Hochstein S, Shapley RM (1976) Linear and nonlinear spatial subunits in Y cat retinal
1209 ganglion cells. *J Physiol* 262:265–284.
- 1210 Idrees S, Baumann MP, Franke F, Münch TA, Hafed ZM (2020) Perceptual saccadic
1211 suppression starts in the retina. *Nat Commun* 11:1977.
- 1212 Karamanlis D, Gollisch T (2021) Nonlinear Spatial Integration Underlies the Diversity of
1213 Retinal Ganglion Cell Responses to Natural Images. *J Neurosci* 41:3479–3498.
- 1214 Karamanlis D, Schreyer HM, Gollisch T (2022) Retinal Encoding of Natural Scenes. *Annu*
1215 *Rev Vis Sci* 8:171–193.
- 1216 Khuc-Trong P, Rieke F (2008) Origin of correlated activity between parasol retinal ganglion
1217 cells. *Nat Neurosci* 11:1343–1351.
- 1218 Kolb H, Famiglietti EV (1974) Rod and Cone Pathways in the Inner Plexiform Layer of Cat
1219 Retina. *Science* 186:47–49.

- 1220 Krishnamoorthy V, Weick M, Gollisch T (2017) Sensitivity to image recurrence across eye-
 1221 movement-like image transitions through local serial inhibition in the retina. *eLife*
 1222 6:e22431.
- 1223 Kuo SP, Schwartz GW, Rieke F (2016) Nonlinear spatiotemporal integration by electrical and
 1224 chemical synapses in the retina. *Neuron* 90:320–332.
- 1225 Lamb TD (1995) Photoreceptor Spectral Sensitivities: Common Shape in the Long-
 1226 wavelength Region. *Vision Res* 35:3083–3091.
- 1227 Land MF (1999) Motion and vision: why animals move their eyes. *J Comp Physiol A*
 1228 185:341–352.
- 1229 Lettvin JY, Maturana HR, McCulloch WS, Pitts WH (1959) What the Frog's Eye Tells the
 1230 Frog's Brain. *Proc IRE* 47:1940–1951.
- 1231 Liu B, Hong A, Rieke F, Manookin MB (2021) Contribution of linear and nonlinear
 1232 mechanisms to predictive motion estimation. *bioRxiv* 2021.11.09.467979.
 1233 <https://doi.org/10.1101/2021.11.09.467979>.
- 1234 Manookin MB, Beaudoin DL, Ernst ZR, Flagel LJ, Demb JB (2008) Disinhibition Combines
 1235 with Excitation to Extend the Operating Range of the OFF Visual Pathway in
 1236 Daylight. *J Neurosci* 28:4136–4150.
- 1237 Manookin MB, Patterson SS, Linehan CM (2018) Neural mechanisms mediating motion
 1238 sensitivity in parasol ganglion cells of the primate retina. *Neuron* 97:1327-1340.e4.
- 1239 Masland RH (2012) The tasks of amacrine cells. *Vis Neurosci* 29:3–9.
- 1240 Masri RA, Percival KA, Koizumi A, Martin PR, Grünert U (2019) Survey of retinal ganglion
 1241 cell morphology in marmoset. *J Comp Neurol* 527:236–258.
- 1242 McMahon MJ, Packer OS, Dacey DM (2004) The Classical Receptive Field Surround of
 1243 Primate Parasol Ganglion Cells Is Mediated Primarily by a Non-GABAergic Pathway.
 1244 *J Neurosci* 24:3736–3745.
- 1245 Menger N, Pow DV, Wässle H (1998) Glycinergic Amacrine Cells of the Rat Retina. *J Comp*
 1246 *Neurol* 401:34–46.
- 1247 Molnar A, Werblin F (2007) Inhibitory Feedback Shapes Bipolar Cell Responses in the
 1248 Rabbit Retina. *J Neurophysiol* 98:3423–3435.
- 1249 Noda H, Adey WR (1974) Retinal ganglion cells of the cat transfer information on saccadic
 1250 eye movement and quick target motion. *Brain Res* 70:340–345.
- 1251 Pachitariu M, Steinmetz NA, Kadir SN, Carandini M, Harris KD (2016) Fast and accurate
 1252 spike sorting of high-channel count probes with KiloSort. *Adv Neural Inf Process Syst*
 1253 29:4448–4456.
- 1254 Peng Y-R, Shekhar K, Yan W, Herrmann D, Sappington A, Bryman GS, van Zyl T, Do MTH,
 1255 Regev A, Sanes JR (2019) Molecular Classification and Comparative Taxonomics of
 1256 Foveal and Peripheral Cells in Primate Retina. *Cell* 176:1222–1237.

- 1257 Pourcho RG, Goebel DJ (1985) A Combined Golgi and Autoradiographic Study of
 1258 (³H)Glycine-Accumulating Amacrine Cells in the Cat Retina. *J Comp Neurol*
 1259 233:473–480.
- 1260 Protti DA, Di Marco S, Huang JY, Vonhoff CR, Nguyen V, Solomon SG (2014) Inner retinal
 1261 inhibition shapes the receptive field of retinal ganglion cells in primate. *J Physiol*
 1262 592:49–65.
- 1263 Rhoades CE, Shah NP, Manookin MB, Brackbill N, Kling A, Goetz G, Sher A, Litke AM,
 1264 Chichilnisky EJ (2019) Unusual Physiological Properties of Smooth Monostratified
 1265 Ganglion Cell Types in Primate Retina. *Neuron* 103:658–672.
- 1266 Rosa JM, Ruele S, Ding H, Lagnado L (2016) Crossover Inhibition Generates Sustained
 1267 Visual Responses in the Inner Retina. *Neuron* 90:308–319.
- 1268 Roska B, Werblin F (2003) Rapid global shifts in natural scenes block spiking in specific
 1269 ganglion cell types. *Nat Neurosci* 6:600–608.
- 1270 Schiller PH (1992) The ON and OFF channels of the visual system. *Trends Neurosci* 15:86–
 1271 92.
- 1272 Schnapf JL, Nunn BJ, Meister M, Baylor DA (1990) Visual transduction in cones of the
 1273 monkey macaca fascicularis. *J Physiol* 427:681–713.
- 1274 Schneeweis DM, Schnapf JL (1995) Photovoltage of Rods and Cones in the Macaque Retina.
 1275 *Science* 268:1053–1056.
- 1276 Schottdorf M, Lee BB (2021) A quantitative description of macaque ganglion cell responses
 1277 to natural scenes: the interplay of time and space. *J Physiol* 599:3169–3193.
- 1278 Schwartz G, Rieke F (2011) Nonlinear spatial encoding by retinal ganglion cells: when $1 + 1$
 1279 $\neq 2$. *J Gen Physiol* 138:283–290.
- 1280 Segev R, Schneidman E, Goodhouse J, Berry MJ (2007) Role of Eye Movements in the
 1281 Retinal Code for a Size Discrimination Task. *J Neurophysiol* 98:1380–1391.
- 1282 Sivyer B, Tomlinson A, Taylor WR (2019) Simulated Saccadic Stimuli Suppress ON-Type
 1283 Direction-Selective Retinal Ganglion Cells via Glycinergic Inhibition. *J Neurosci*
 1284 39:4312–4322.
- 1285 Slaughter MM, Miller RF (1981) 2-Amino-4-Phosphonobutyric Acid: A New
 1286 Pharmacological Tool for Retina Research. *Science* 211:182–185.
- 1287 Takeshita D, Gollisch T (2014) Nonlinear Spatial Integration in the Receptive Field Surround
 1288 of Retinal Ganglion Cells. *J Neurosci* 34:7548–7561.
- 1289 Tovée MJ, Bowmaker JK, Mollon JD (1992) The Relationship Between Cone Pigments and
 1290 Behavioural Sensitivity in a New World Monkey (*Callithrix jacchus jacchus*). *Vision*
 1291 *Res* 32:867–878.
- 1292 Travis DS, Bowmaker JK, Mollon JD (1988) Polymorphism of visual pigments in a
 1293 callitrichid monkey. *Vision Res* 28:481–490.

- 1294 Troilo D, Howland HC, Judge SJ (1993) Visual Optics and Retinal Cone Topography in the
1295 Common Marmoset (*Callithrix jacchus*). *Vision Res* 33:1301–1310.
- 1296 Turner MH, Rieke F (2016) Synaptic Rectification Controls Nonlinear Spatial Integration of
1297 Natural Visual Inputs. *Neuron* 90:1257–1271.
- 1298 Wässle H, Boycott BB (1991) Functional Architecture of the Mammalian Retina. *Physiol Rev*
1299 71:447–480.
- 1300 Wässle H, Grünert U, Chun M-H, Boycott BB (1995) The Rod Pathway of the Macaque
1301 Monkey Retina: Identification of All-Amacrine Cells With Antibodies Against
1302 Calretinin. *J Comp Neurol* 361:537–551.
- 1303 Werblin FS (2010) Six different roles for crossover inhibition in the retina: Correcting the
1304 nonlinearities of synaptic transmission. *Vis Neurosci* 27:1–8.
- 1305 Wienbar S, Schwartz GW (2018) The dynamic receptive fields of retinal ganglion cells. *Prog*
1306 *Retin Eye Res* 67:102–117.
- 1307 Wurtz RH (2008) Neuronal mechanisms of visual stability. *Vision Res* 48:2070–2089.
- 1308 Yarbus AL (1967) *Eye Movements and Vision*. New York: Plenum Press.
- 1309 Yu Z, Turner MH, Baudin J, Rieke F (2022) Adaptation in cone photoreceptors contributes to
1310 an unexpected insensitivity of primate On parasol retinal ganglion cells to spatial
1311 structure in natural images. *eLife* 11:e70611.
- 1312 Zaghoul KA, Boahen K, Demb JB (2003) Different Circuits for ON and OFF Retinal
1313 Ganglion Cells Cause Different Contrast Sensitivities. *J Neurosci* 23:2645–2654.
- 1314 Zapp SJ, Nitsche S, Gollisch T (2022) Retinal receptive-field substructure: scaffolding for
1315 coding and computation. *Trends Neurosci* 45:430–445.

1316 **Figure Captions**

1317 **Figure 1.** Sample ganglion cell responses to saccade-like grating shifts. (A) Schematic
1318 representation of the stimulus, consisting of a sequence of 533-ms fixations of a square-wave
1319 grating at one of four possible positions (spatial phases) and brief transitions over 67 ms. The
1320 transition either occurred via a rapid motion of the grating or via a gray-screen mask at mean
1321 luminance. The sequence of fixation positions and the type of transition were randomized. (B)
1322 Responses of three sample ganglion cells to different combinations of grating position before
1323 and after the transition. Top row shows raster plots for both gray (red) and motion (blue)
1324 transitions, bottom row shows the corresponding PSTHs. Shaded areas mark the transition
1325 periods. (C) PSTHs of the sample cells for all 16 possible combinations of grating positions
1326 before the transition (starting position) and after the transition (target position). Here,

1327 responses to gray-screen and motion transitions were pooled. (D) Similarity of responses to
 1328 gray and motion transitions for all cells included in the analysis. The similarity measure R_{norm}^2
 1329 was calculated as the modified coefficient of determination between responses to gray and to
 1330 motion, normalized by the corresponding coefficient for odd versus even trials (independent
 1331 of the transition type). Nearly all R_{norm}^2 values are larger than 0.5, indicating high similarity
 1332 between the responses to gray and motion transition.

1333 **Figure 2.** Analysis of ganglion cell sensitivity. (A) PSTH of a sample cell (Cell 2 from Fig 1)
 1334 for the transition between Position 3 and Position 1, smoothed by a Gaussian filter. (In the
 1335 quantitative analysis, the two response windows were smoothed separately.) Dashed vertical
 1336 lines mark the boundaries of the first and second response windows. For each response
 1337 window, the peak response is identified as depicted by the red crosses and arrows. (B) The
 1338 response matrices contain the peak response during the first window (left) and second window
 1339 (right) for all combinations of starting and target position, depicted here in a color-coded
 1340 fashion with brighter colors denoting stronger responses. The dashed squares indicate the
 1341 entries that correspond to the sample PSTH shown in (A). (C) Fourier transformations of the
 1342 response matrices. The entries of the transformed matrices quantify patterns in the response
 1343 matrices. Entries that are highlighted by dashed squares correspond to relevant patterns in the
 1344 response matrix, which are depicted schematically below the Fourier transformed matrices.
 1345 For the sample cell, the yellow (0, 1) entry of the first and the yellow (1, 0) entry of the
 1346 second Fourier transformed response matrix reflect the start and target sensitivity of the cell.
 1347 (D) Scatterplot of the start, target, and change sensitivity of the first response window for each
 1348 cell. The large yellow data point marks the sample cell from (A-C). (E) Same for the
 1349 sensitivity of the second response window. (F) Elements of the final sensitivity vector for
 1350 each cell, obtained by combining the start sensitivity of the first response window and the
 1351 target and change sensitivity of the second response window.

1352 **Figure 3.** Classification of retinal ganglion cells of a sample experiment. (A) Scatterplot of
 1353 the effective receptive-field diameter versus the projection onto the first principal component
 1354 of the temporal filter for all classified cells (magenta: On parasol cells, green: On midget
 1355 cells, red: Off parasol cells, blue: Off midget cells, orange: Large Off cells). (B) Same as (A),
 1356 but for second principal component versus first principal component of the temporal filter.
 1357 (C) Autocorrelation functions, receptive field layouts (1.5-sigma ellipses of receptive-field
 1358 Gaussians; distant cells excluded), temporal filters, nonlinearities (scaled to the same
 1359 maximum) of all classified cells, and a sample spatial filter, grouped by cell type.

1360 **Figure 4.** Coding properties of ganglion cell types. (A) PSTHs of different sample cells,
1361 showing the responses of the cells to all 16 combinations of starting and target position.
1362 Shaded regions denote the transition period and dashed vertical lines mark the borders of the
1363 response windows used for analysis. (B) Sensitivity vectors of all cells of the five
1364 distinguished cell types. (C) Boxplots of the distributions of sensitivity measures (entries of
1365 the sensitivity vector) for each of the five cell types. Boxes denote the central 50% of data
1366 points (i.e., from 25% to 75%), whiskers the central 90% (from 5% to 95%), and horizontal
1367 lines inside the boxes the medians.

1368 **Figure 5.** Dependence of stimulus sensitivities on receptive field size. (A) Sensitivity to the
1369 starting position versus width of the receptive field for all On cells. Receptive field width was
1370 defined as the extent in x-direction (perpendicular to the grating) of the 1.5-sigma ellipse of
1371 the receptive-field Gaussian and given relative to the size of a grating bar. Circles represent
1372 individual cells, solid lines are robust linear regressions for each cell type using the Theil-Sen
1373 estimator. (B) Same as in (A) but for sensitivity to the target position. (C) Same as in (A) but
1374 for sensitivity to change. (D)-(F) Same as in (A)-(C) but for Off cells.

1375 **Figure 6.** Comparison of saccade responses with responses to flashed gratings.
1376 (A) Exemplary saccade responses depicted as in Fig 4A. Large Off cell is Cell 3 from Fig 1C.
1377 (B) PSTHs of the cells in (A) in response to offset and onset of the grating stimulus. Shown is
1378 the average of the 60 μm and 120 μm bar width responses. The relevant part of the grating
1379 stimulus is schematically depicted beneath each PSTH. Dashed box marks the part of the
1380 response used to determine the response strength. Scale bars of (A) apply here, too. (C)
1381 Relative strength of the response to the onset of the grating versus its offset (y axis) and
1382 relative sensitivity to the target versus starting position during the saccadic stimulus (x axis).
1383 Values close to 1 represent a dominant onset response/target sensitivity, values close to -1 a
1384 dominant offset response/start sensitivity. Colors denote cell types, stars represent means of
1385 the cell types. (D) Average response strength of all On parasol/midget cells in response to the
1386 onset/offset of the grating, depending on the grating's bar width (logarithmic axis). Response
1387 strengths are normalized to the same maximum before averaging over the cells. (E) Same as
1388 (D) but for Off cells.

1389 **Figure 7.** Modeling ganglion cell responses to saccades based on responses to brightness
1390 steps. (A) Exemplary PSTHs for all five retinal ganglion cell types to full-field brightness
1391 steps. The stimulus is schematically depicted beneath each PSTH. (B) Schematic depiction of
1392 obtaining a response prediction for the ON parasol cell in (A). The cell's response to the full-

1393 field brightness steps (top) was split into responses to the on- and offsets of white and black
1394 (zoomed-in insets below, small circles and coloring of the PSTHs denote the brightness
1395 change). For the linear model (left), the response to an offset of the first grating was estimated
1396 by scaling the cell's response to the offset of the appropriate brightness step, here one third of
1397 the offset of white, corresponding to the relative decrease in mean luminance inside the
1398 receptive field. Analogously, the response to the onset of the new grating was estimated here
1399 as one third of the onset of white, corresponding to the increase in mean brightness. Unlike
1400 depicted here, these two response components overlapped strongly, because of the briefness
1401 of the transition. They were then summed to form the final response prediction. For the
1402 nonlinear model (right), each pixel directly contributed response components to the final
1403 response thereby omitting the averaging of the brightness inside the receptive field. At the
1404 offset of the first grating in this example, one third of the receptive field turned from black to
1405 gray and two thirds from white to gray, yielding a one-third contribution of the black offset
1406 response and a two-thirds contribution of the white offset response. The onset of the second
1407 grating position was treated analogously and the four response components were summed to
1408 generate the final response prediction.

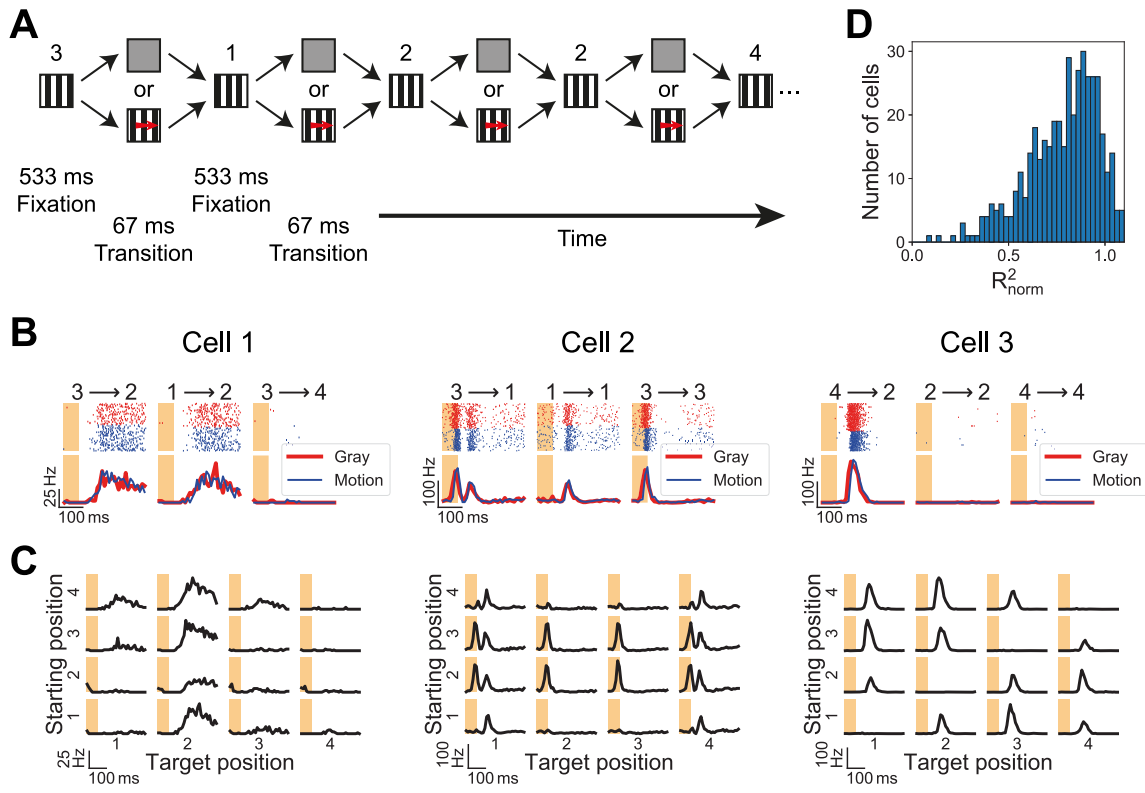
1409 **Figure 8.** Model evaluation for On parasol (left) and On midget (right) cells. (A) PSTHs of
1410 sample cells to the full-field brightness steps. The On midget cell is same cell as in Fig 6A.
1411 (B) Experimental responses to the saccadic stimulus (thin black line with gray filling) and
1412 predictions by the linear model (thick blue line) of the same sample cells to the saccadic
1413 stimulus. Layout of the plot is the same as in Fig 1C. (C) Same as (B) but for the nonlinear
1414 model (red line). (D) Illustrations of the content of the cells' receptive fields at the four
1415 grating positions. (E) Modified coefficient of determination R^2 for the response matrix of the
1416 data versus the linear model (x axis) and versus the nonlinear model (y axis). R^2 values are
1417 shown separately for the first and second response matrix. Colored dots represent all ganglion
1418 cells of the column's cell type, light gray dots all other cell types. Cells with a model R^2
1419 below -0.05 have been plotted on the axis. (F) Distributions of the distances between modeled
1420 and experimental sensitivity vectors for the linear and the nonlinear model.

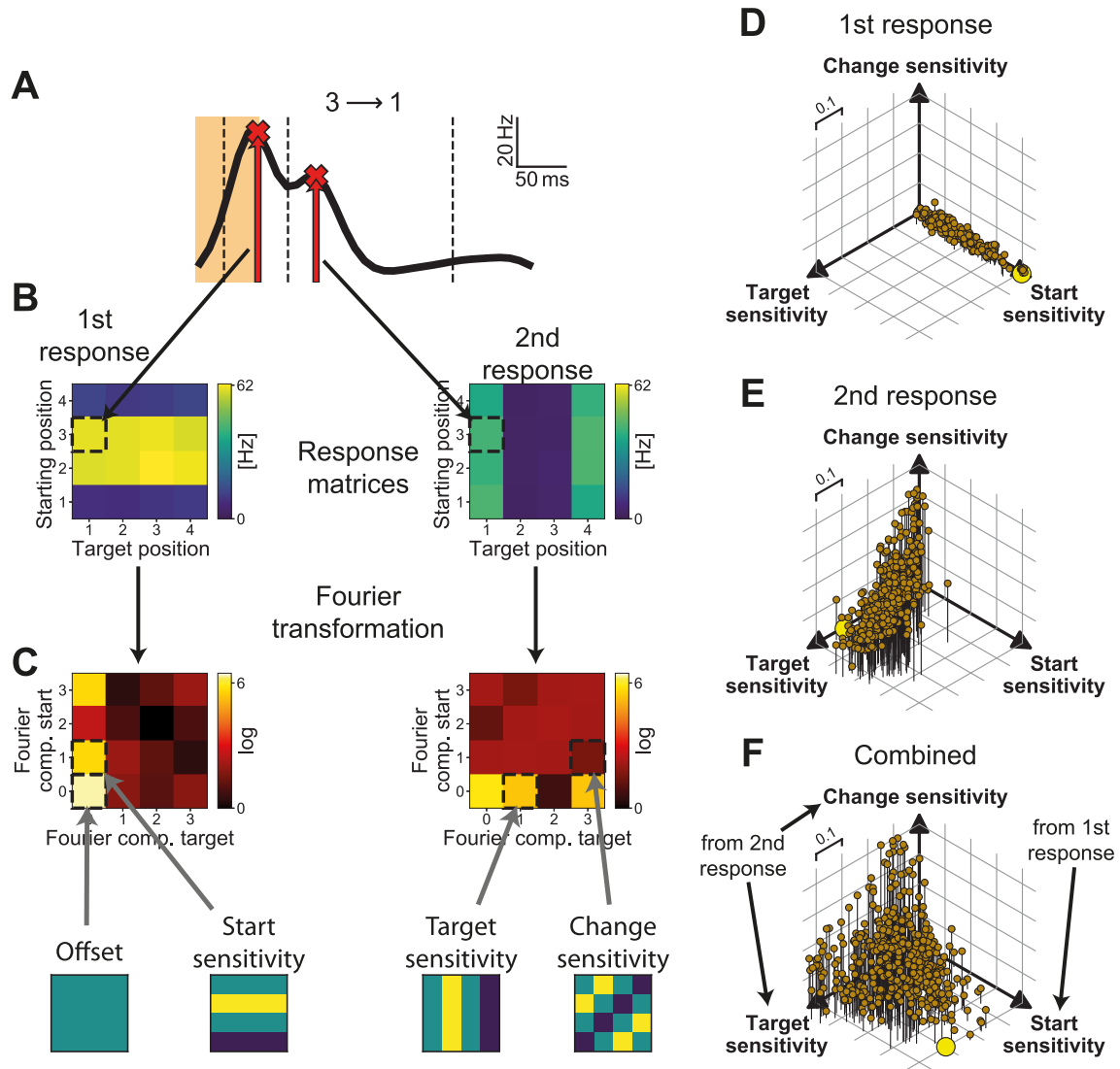
1421 **Figure 9.** Model evaluation for Off cells. Same layout and subfigures as in Fig 8, but with Off
1422 parasol cells in the left column, Off midget cells in the middle column, and Large Off cells in
1423 the right column.

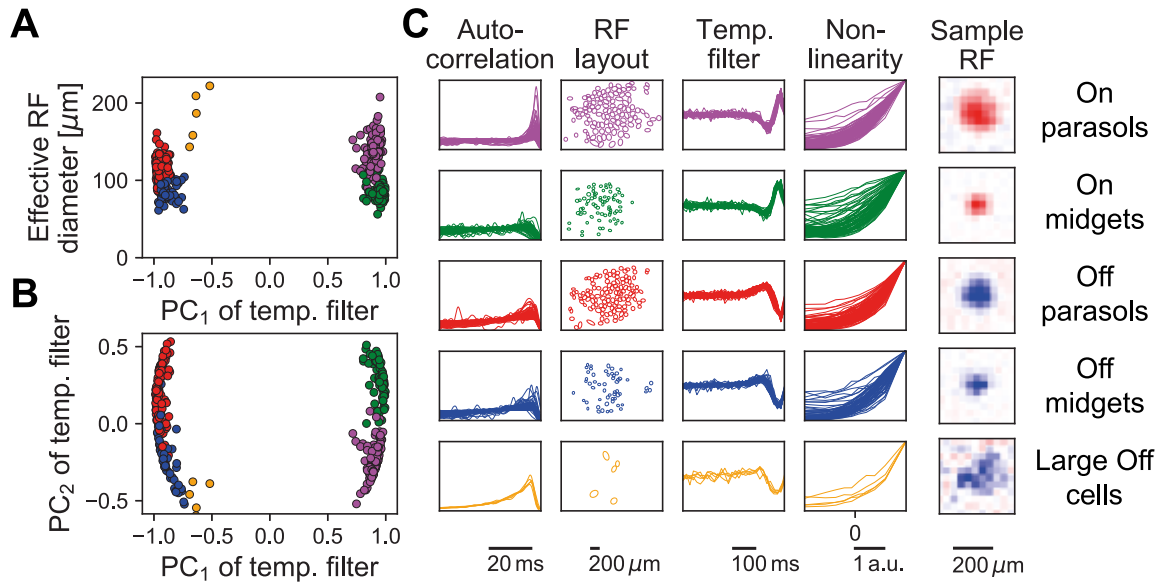
1424 **Figure 10.** Influence of receptive field size on model predictions. (A) Mean start sensitivity of
1425 each On cell type as modeled by the linear (dashed line) and nonlinear (solid line) model,

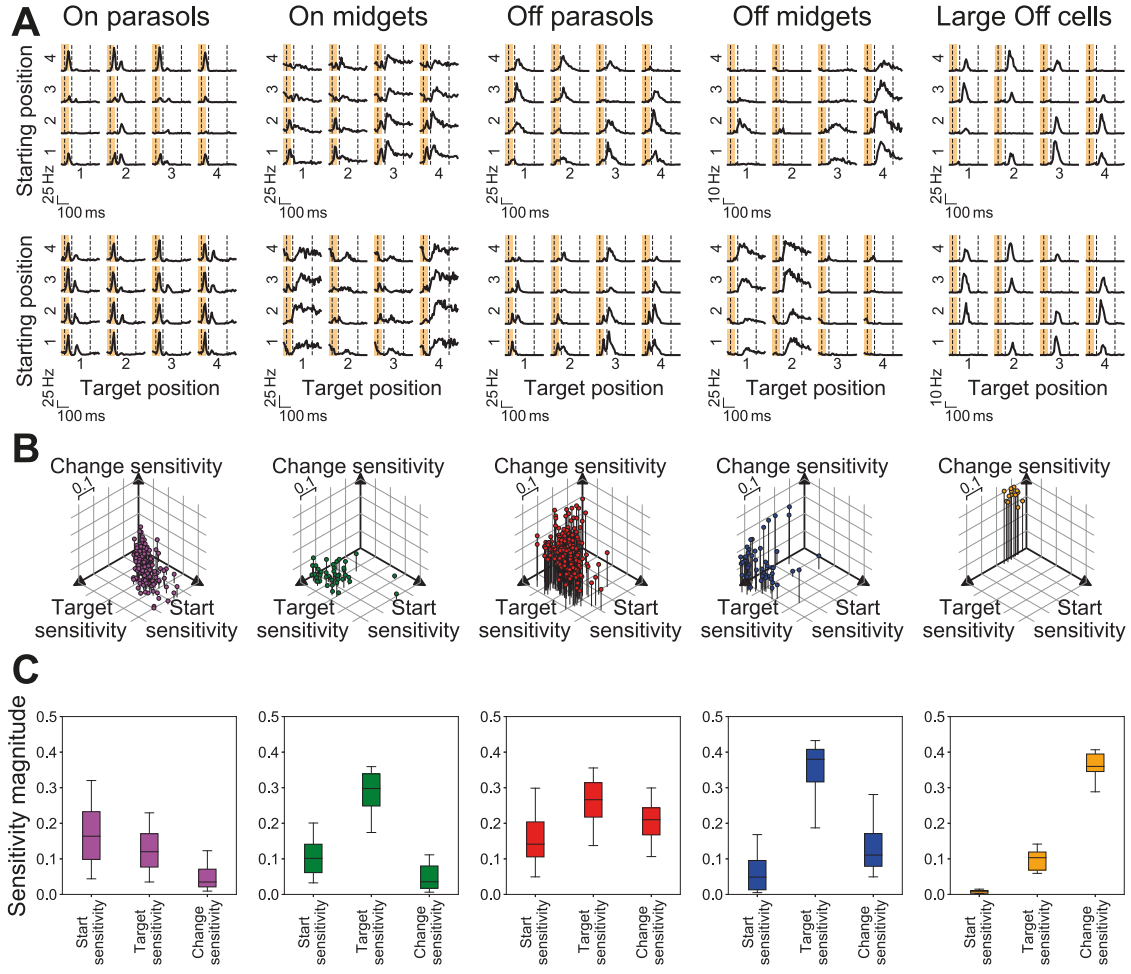
1426 depending on the receptive field width each cell was scaled to. Receptive field width was
1427 defined as in Fig 5. Measured cells are plotted in the background for reference. (B) Same as
1428 (A) but for target sensitivity. (C) Same as (A) but for change sensitivity. (D) – (E) Same as
1429 (A) – (C) but for Off cells.

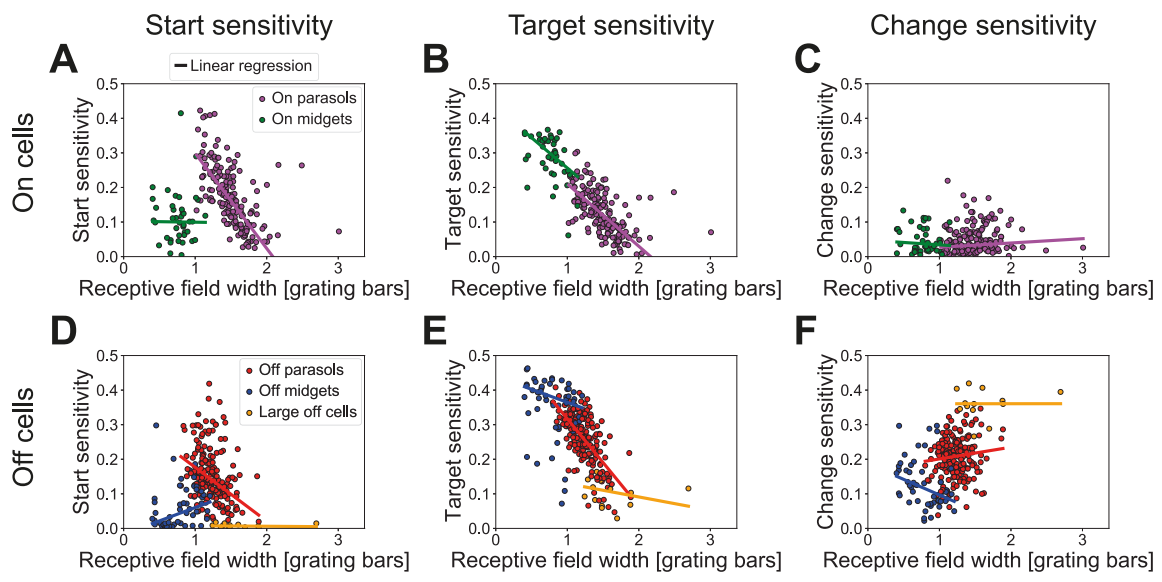
1430 **Figure 11.** Sensitivity vectors from models and experiments. (A) Boxplots for the distribution
1431 of start-sensitivity values for each cell type, obtained via each of the two models and from the
1432 experimental data. The box marks the central 50%, whiskers the central 90%, and the
1433 horizontal line inside the box the median. (B) Same as (A) but for target sensitivity. (C) Same
1434 as (A) but for sensitivity to grating position change. (D) Scatter plot of sensitivity vectors
1435 calculated from the linear model for all cells of the five types. (E) Same as (D) but for
1436 nonlinear models. (F) Same as (D) but for experimental data.

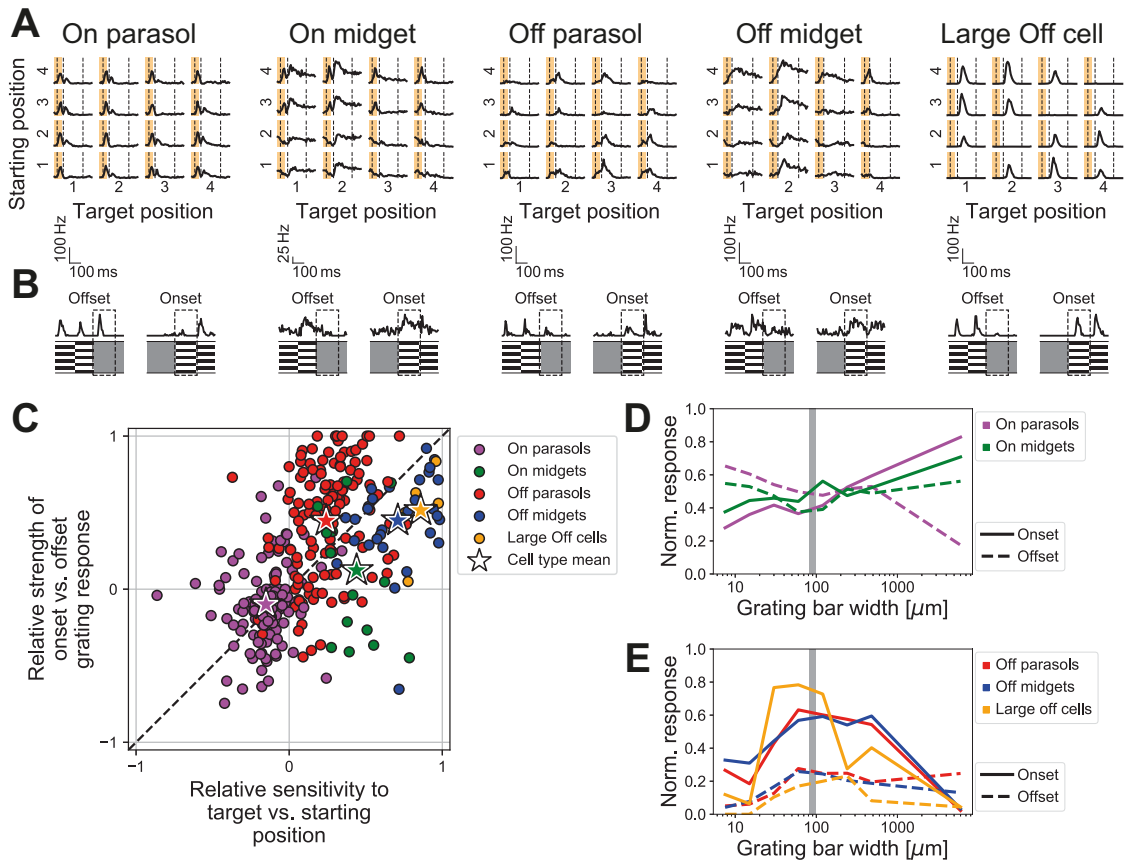


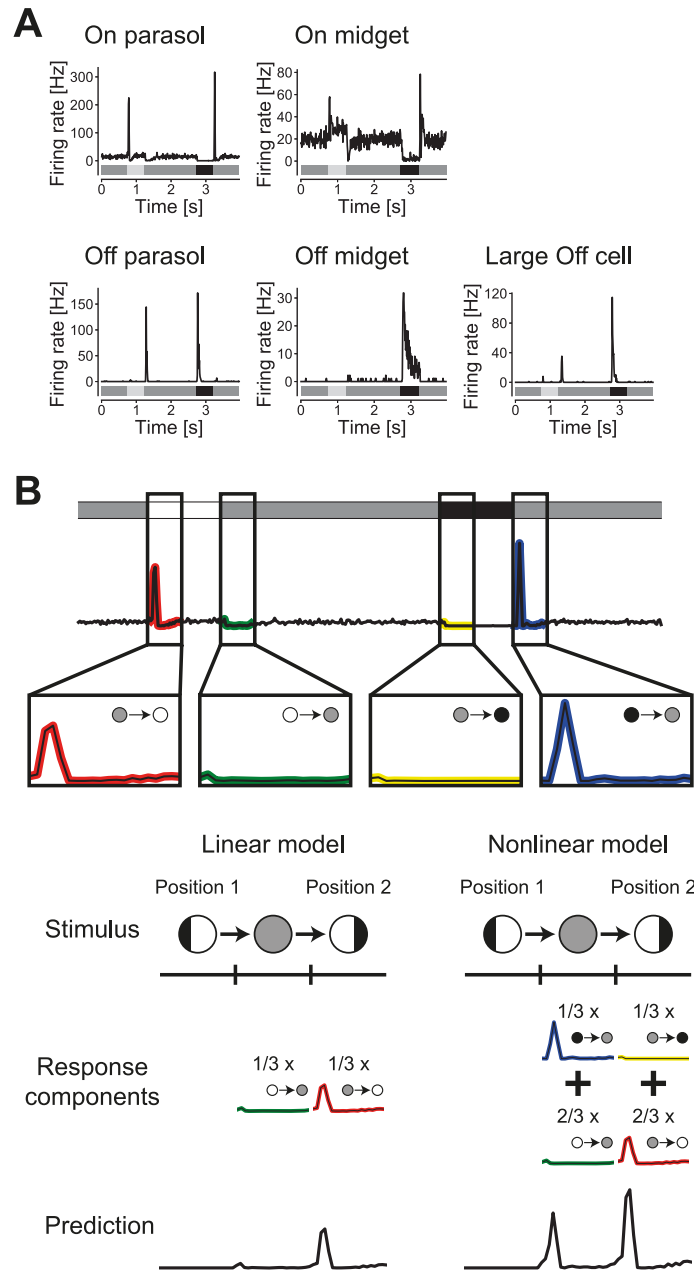


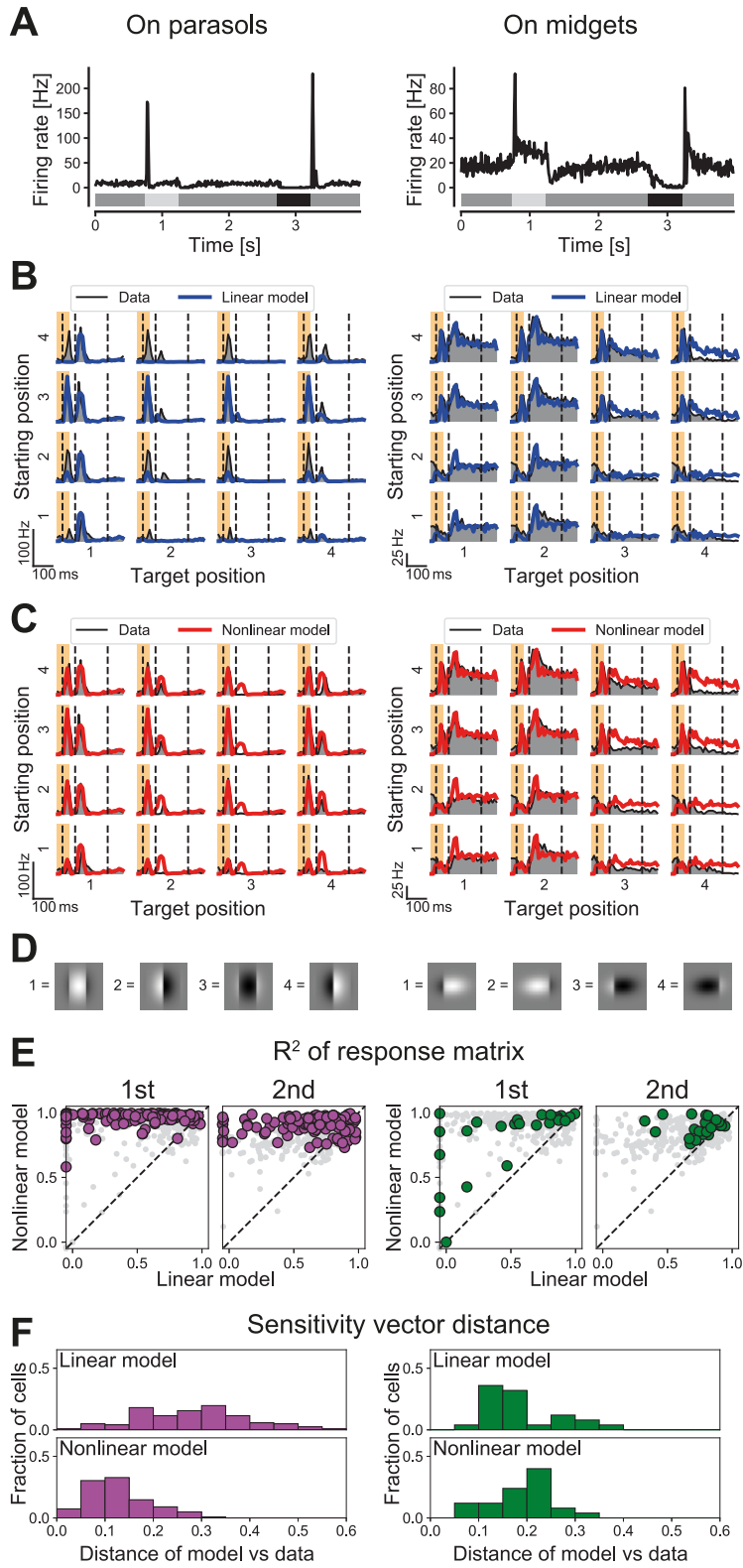


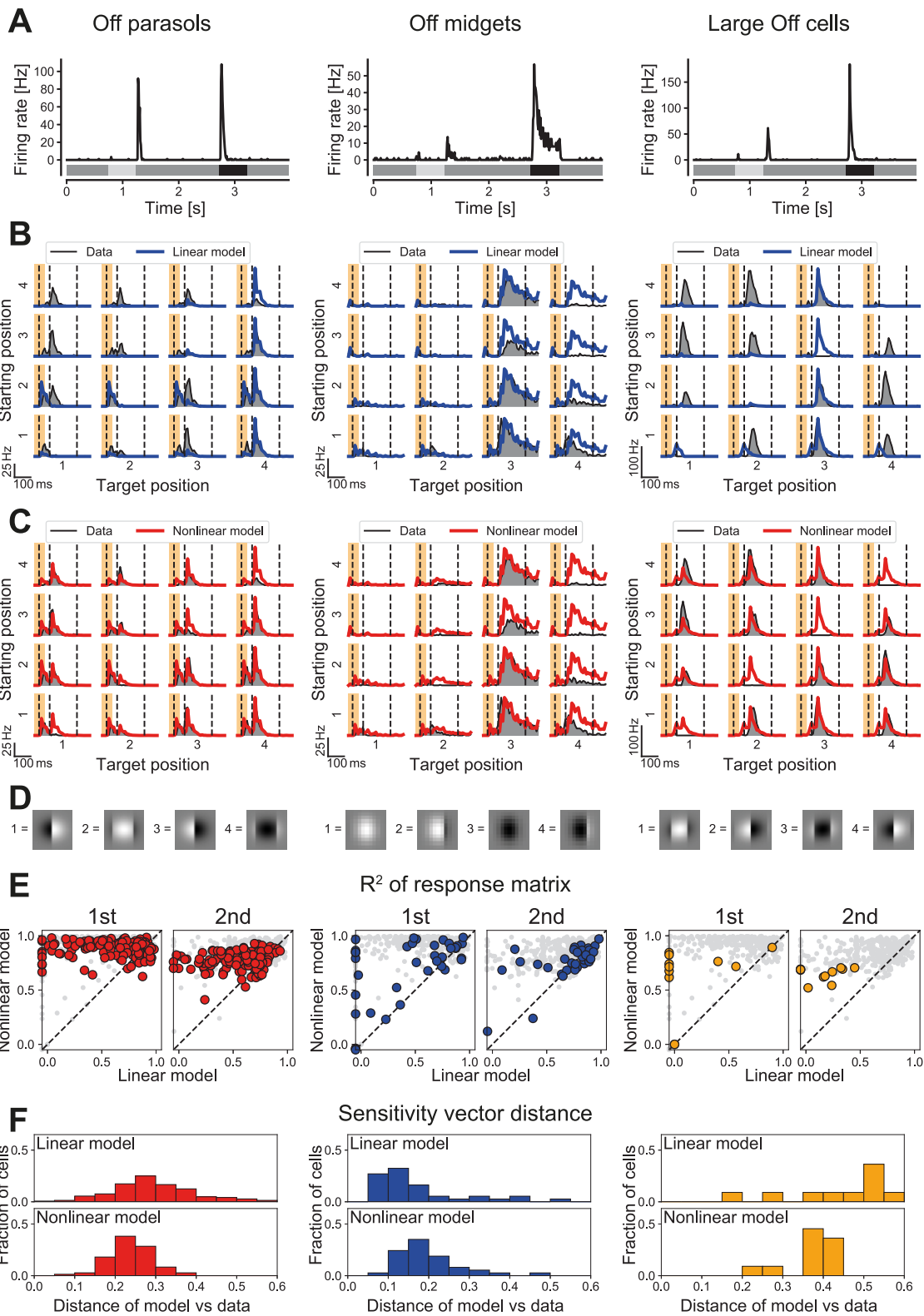


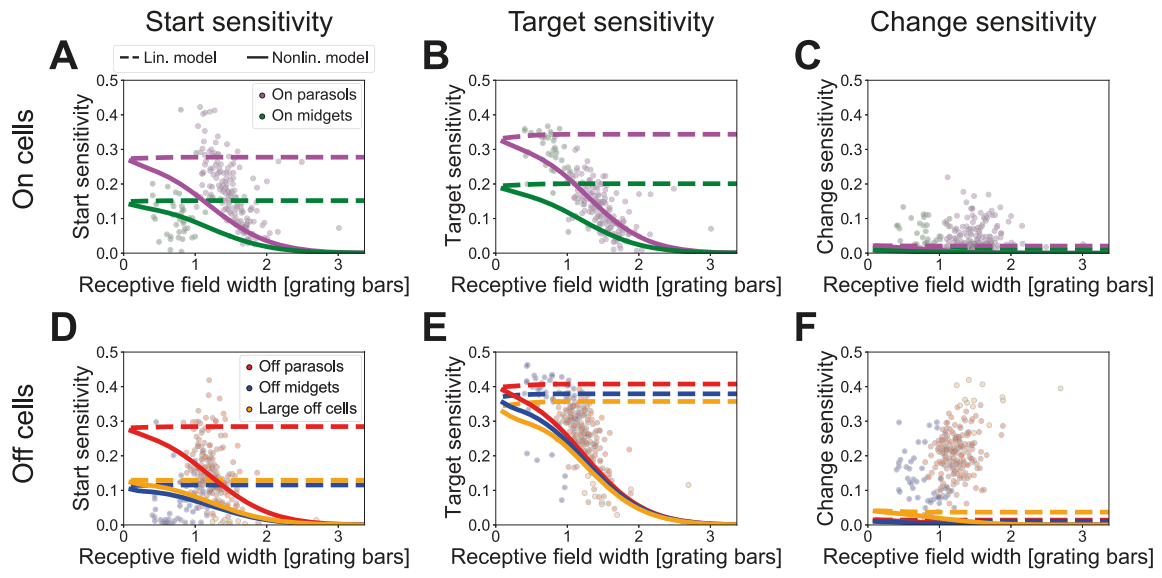




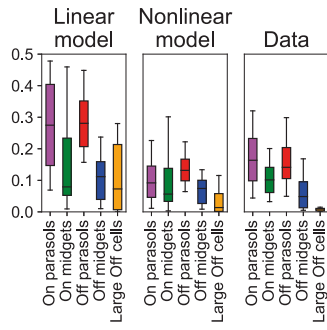




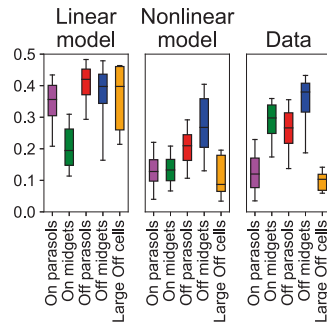




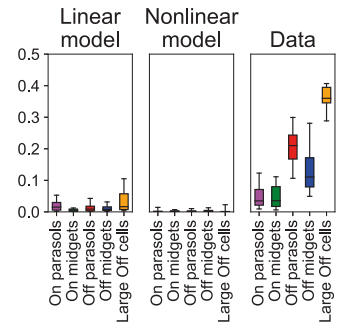
A Start sensitivity



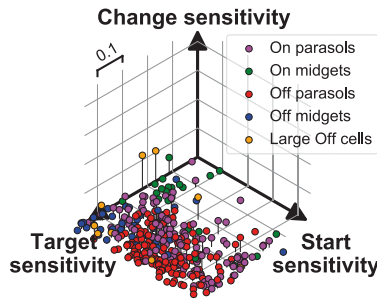
B Target sensitivity



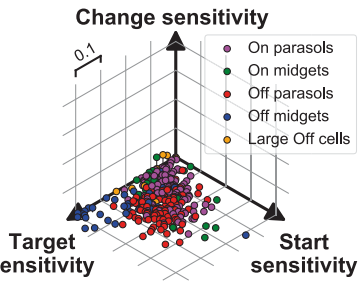
C Change sensitivity



D Linear model



E Nonlinear model



F Data

